Published in : Journal of Agricultural and Food Chemistryl (2024), vol. 72, n°37, pp. 20670-20678
DOI: 10.1021/acs.jafc.4c05094
Status : Postprint (Author's version)

DEVELOPMENT OF LIGANDS FOR THE SUPER CONSERVED ORPHAN G PROTEINCOUPLED RECEPTOR GPR27 WITH IMPROVED EFFICACY AND POTENCY

Thanigaimalai Pillaiyar,*,¶ Monika Wozniak,¶ Dayana Abboud, Alexander Rasch, Aenne-Dorothea Liebing, Antti Poso, Thales Kronenberger, Claudia Stäubert, Stefan A. Laufer, and Julien Hanson*

Corresponding Authors

Thanigaimalai Pillaiyar − Institute of Pharmacy, Pharmaceutical/Medicinal Chemistry and Tübingen Center for Academic Drug Discovery, Eberhard Karls University Tübingen, 72076 Tübingen, Germany; orcid.org/00000001-5575-8896; Email: thanigaimalai.pillaiyar@unituebingen.de

Julien Hanson − Laboratory of Molecular Pharmacology, GIGA-Molecular Biology of Diseases, University of Liege, B4000 Liège, Belgium; Laboratory of Medicinal Chemistry, Centre for Interdisciplinary Research on Medicines (CIRM), University of Liège, B-4000 Liège Belgium; Phone: +32 4 366 4748; Email: j.hanson@uliege.be

Authors

Monika Wozniak − Laboratory of Molecular Pharmacology, GIGA-Molecular Biology of Diseases, University of Liège, B-4000 Liege, Belgium

Dayana Abboud − Laboratory of Molecular Pharmacology, GIGA-Molecular Biology of Diseases, University of Liège, B-4000 Liège, Belgium

Alexander Rasch − Institute of Pharmacy, Pharmaceutical/Medicinal Chemistry and Tübingen Center for Academic Drug Discovery, Eberhard Karls University Tübingen, 72076 Tübingen, Germany

Aenne-Dorothea Liebing − Rudolf Schönheimer Institute of Biochemistry, Faculty of Medicine, Leipzig University, 04103 Leipzig, Germany

Antti Poso − Institute of Pharmacy, Pharmaceutical/Medicinal Chemistry and Tübingen Center for Academic Drug Discovery, Eberhard Karls University Tübingen, 72076 Tübingen, Germany; Cluster of Excellence iFIT (EXC 2180) "Image-Guided & Functionally Instructed Tumor Therapies", University of Tübingen, 72076 Tübingen, Germany; School of Pharmacy, Faculty of Health Sciences, University of Eastern Finland, 70211 Kuopio, Finland; orcid.org/0000-0003-4196-4204

Thales Kronenberger − Institute of Pharmacy, Pharmaceutical/Medicinal Chemistry and Tübingen Center for Academic Drug Discovery, Eberhard Karls University Tübingen, 72076 Tübingen, Germany; Cluster of

Published in : Journal of Agricultural and Food Chemistryl (2024), vol. 72, n°37, pp. 20670-20678
DOI: 10.1021/acs.jafc.4c05094
Status : Postprint (Author's version)

Excellence iFIT (EXC 2180) "Image-Guided & Functionally Instructed Tumor Therapies", University of Tübingen, 72076 Tübingen, Germany; School of Pharmacy, Faculty of Health Sciences, University of Eastern Finland, 70211 Kuopio, Finland

Claudia Stäubert − Rudolf Schönheimer Institute of Biochemistry, Faculty of Medicine, Leipzig University, 04103

Leipzig, Germany

Stefan A. Laufer − Institute of Pharmacy, Pharmaceutical/ Medicinal Chemistry and Tübingen Center for Academic Drug Discovery, Eberhard Karls University Tübingen, 72076 Tübingen, Germany; Cluster of Excellence iFIT (EXC 2180) "Image-Guided & Functionally Instructed Tumor Therapies", University of Tübingen, 72076 Tübingen, Germany; orcid.org/0000-0001-6952-1486

Complete contact information is available at: https://pubs.acs.org/10.1021/acs.jmedchem.3c02030

Abstract

The orphan G protein-coupled receptor GPR27 appears to play a role in insulin production, secretion, lipid metabolism, neuronal plasticity, and l-lactate homeostasis. However, investigations on the function of GPR27 are impaired by the lack of potent and efficacious agonists. We describe herein the development of di- and trisubstituted benzamide derivatives 4a-e, 7a-z, and 7aa-ai, which display GPR27-specific activity in a β-arrestin 2 recruitment-based assay. Highlighted compounds are PT-91 (7p: pEC_{50} 6.15; E_{max} 100%) and 7ab (pEC_{50} 6.56; E_{max} 99%). A putative binding mode was revealed by the docking studies of 7p and 7ab with a GPR27 homology model. The novel active compounds exhibited no GPR27-mediated activation of G proteins, indicating that the receptor may possess an atypical profile. Compound 7p displays high metabolic stability and brain exposure in mice. Thus, 7p represents a novel tool to investigate the elusive pharmacology of GPR27 and assess its potential as a drug target.

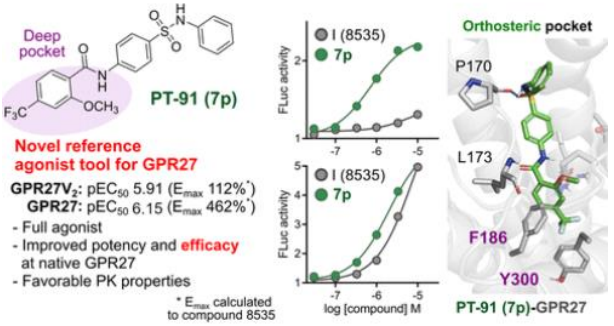

Published in : Journal of Agricultural and Food Chemistryl (2024), vol. 72, n°37, pp. 20670-20678
DOI: 10.1021/acs.jafc.4c05094
Status : Postprint (Author's version)

Introduction

The most prevalent superfamily of integral membrane proteins in mammals is the G protein-coupled receptor (GPCR) family, which is characterized by seven transmembrane helices. In humans, nearly 900 genes encode GPCRs, broadly classified as either "physiological" (365 members in humans) or "sensory" receptors (435 members in humans for olfaction, vision, taste, and pheromones).[1] Approximately 35% of marketed drugs exert their therapeutic effect through the direct interaction with a GPCR,[2,3] highlighting the importance of their study for the development of innovative drugs. The International Union of Basic and Clinical Pharmacology classifies around 100 GPCRs as orphan GPCRs, which are defined as receptors without known validated endogenous ligands.[4,5] A detailed examination of the current literature on orphans reveals that the majority of them have received little attention.[6] This is owing, at least in part, to the scarcity of pharmacological tools (such as ligands) available to study them.[4,7]

A small cluster of three orphan receptors has received specific interest due to a strikingly high degree of conservation throughout vertebrate evolution.[8,9] Due to their high level of expression in the central nervous system, this subfamily has been named "super conserved receptors expressed in the brain" (SREB).[10] Three members have been identified: GPR27 (SREB1), GPR85 (SREB2), and GPR173 (SREB3).[10]

GPR27 is expressed in the whole brain but is particularly abundant in the striatum, subthalamic nuclei, hypothalamic supraoptic nucleus, olfactory bulb, and hippocampus, notably the dentate gyrus.[10,11] The high levels of GPR27 expression in the brain, particularly in the hippocampus, suggest a role in neural plasticity.[11] GPR27 has also been detected in peripheral tissues, notably the pancreatic *β*-cells, where it may be involved in insulin secretion and production.[12,13] For example, GPR27 knockdown in the murine pancreatic line MIN-6 leads to reduced insulin promoter activity and glucose-stimulated insulin secretion.[12] Furthermore, GPR27 knockout mice have reduced plasma insulin and mild glucose intolerance.[13] GPR27's function in metabolism has also been explored in nonmammalian vertebrates, such as the zebrafish (*Danio rerio*), where its deletion altered insulin signaling and lipid metabolism.[14,15] More recently, in 3T3 embryonic fibroblasts, GPR27 was shown to be linked to L-lactate homeostasis.[16]

Following a screening campaign of ∼7000 compounds from a diversity-oriented synthesis library, our group has identified small-molecule GPR27 agonists I (8535) and II (7941) (Figure 1) that share a 2,4-dichlorobenzamide sulfonamide scaffold.[17] These hit compounds were selective for GPR27 compared to the other SREBs, GPR85 and GPR173. More recently, we revealed a preliminary structure−activity relationship (SAR) based on the diversification of the 2,4-dichlorobenzamide sulfonamide scaffold.[18]

In the absence of an endogenous ligand and only a very few moderately potent and efficacious GPR27 ligands, many aspects of GPR27's basic pharmacology and function remain unexplored. To fill this knowledge gap and advance our understanding of GPR27 (patho)physiological function as well as validate it as a drug target, potent and efficacious pharmacological tools are needed. In the present work, we build upon our previous SARs of I and report the first superior GPR27 agonists compared to the initial screening hit. Docking studies indicate a potential binding site and led to the design of further improved compounds characterized by a trisubstituted benzamide scaffold. Advanced pharmacological evaluation of GPR27

Published in : Journal of Agricultural and Food Chemistryl (2024), vol. 72, n°37, pp. 20670-20678
DOI: 10.1021/acs.jafc.4c05094
Status : Postprint (Author's version)

assays shows that these next-generation agonists are characterized by markedly higher efficacy compared to that of I. Furthermore, we explored the pharmacology of GPR27 upon activation by these new agonists. We show that more efficacious and potent compounds fail to trigger G protein activation in the presence of GPR27. This observation is in line with previous reports and reinforces the hypothesis that GPR27 is an atypical, β-arrestin-biased receptor.

Figure 1. *Structure of lead compounds* **I** *and* **II**.

Results and discussion

CHEMISTRY.

A total of 40 new final compounds ("disubstituted" series 4a-e and 7a-s and "trisubstituted" series 7t-z and 7aa-ai) were synthesized. The synthetic route for all final compounds is outlined in Schemes 1 and 2. Different substituted carboxylic acid chlorides (2a, b) were prepared from the corresponding commercially available carboxylic acids (1a, b) by reaction with thionyl chloride in DCM under a 2 h reflux. After completion of the reaction, the excess thionyl chloride was removed and subsequently coupled with sulfanilic acid (3a) in the presence of sodium hydroxide for obtaining the product 4a, with 4-(methylsulfonyl)aniline (3b) in the presence of diisopropylethylamine (DIPEA) for 4b, or with different sulfanilamides (3c-e) in the presence of sodium hydrogen carbonate for the corresponding final compounds 4c-e (Scheme 1).

According to the established synthetic procedures,[19−22] the key intermediates 4-amino-*N*-phenylsulfonamide derivatives (3f−i, 3k) were produced. In a nutshell, condensation of commercially available acetamidobenzenesulfonyl chloride (5) with different (hetero)arylamines in the presence of triethylamine in dichloromethane (DCM) produced *N*-acetylprotected sulfonamide derivatives (6a−e). By treating these acetamides with hydrochloric acid under reflux conditions, 4amino-*N*-phenylsulfonamides (3f−i, 3k) were obtained. It should be noted that the intermediate *N*-((4-aminophenyl)sulfonyl)acetamide (3j) was purchased. These sulfonamides (3f−k) were subsequently coupled with a wide variety of differently substituted carboxylic acid chlorides (2a, c−o), which were prepared from the corresponding carboxylic acids (1a, c−o) according to the procedure for the preparation of 2a-b. These coupling reactions were performed in acetone in the presence of sodium hydrogen carbonate at ambient conditions for 12 h. Acetone was removed, and the residue was dissolved in water and filtered to get the crude target compounds that were purified by flash column chromatography for the final compounds 7a-s (Scheme 2).

Published in : Journal of Agricultural and Food Chemistryl (2024), vol. 72, n°37, pp. 20670-20678
DOI: 10.1021/acs.jafc.4c05094
Status : Postprint (Author's version)

Figure 1. *Structure of lead compounds I and II.*

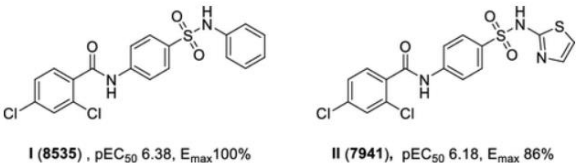

The trisubstituted final compounds 7t-z, 7aa-ah, and 7ai (Scheme 2) were obtained by the reaction of appropriate carboxylic acids (1p-z, 1aa-ae) with sulfonamide 3k in the presence of a 50% solution of 2,4,6-tripropyl-1,3,5,2,4,6trioxatriphosphorinane-2,4,6-trioxide (T3P) solution with ethyl acetate in tetrahydrofuran (THF) at 60 °C for 12 h.

The structures of all synthesized final products were confirmed using ^{1}H and ^{13}C NMR spectra. The purity of all final compounds was determined using high-performance liquid chromatography (HPLC) in combination with UV and electrospray ionization mass spectrometry, which confirmed a purity of >95%.

Scheme 1. *Synthesis of Target Compounds 4a-e*[a]

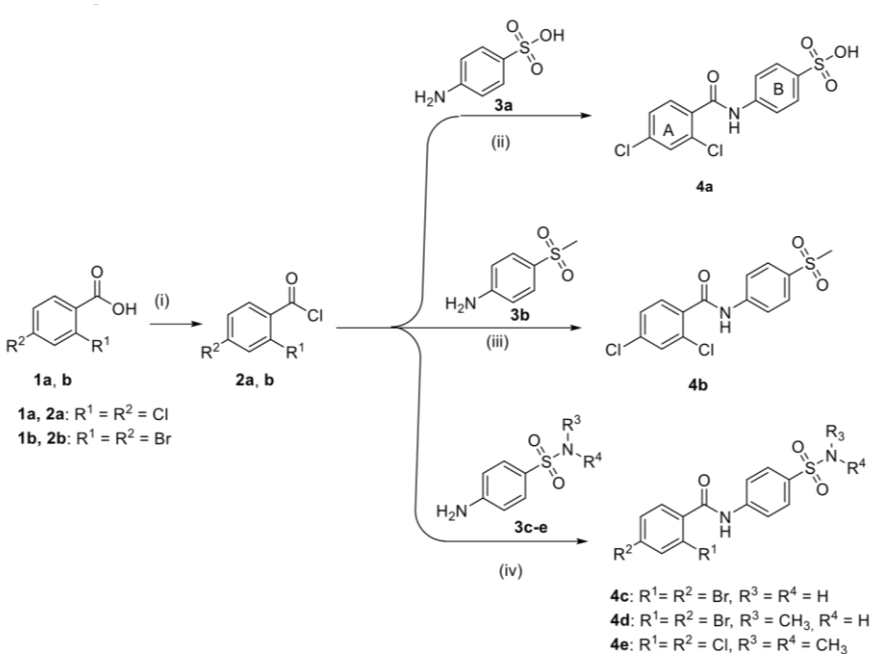

[a]Reagents and conditions: (i) DCM, $SOCl_2$, 50 °C, 1 h; (ii) 5% NaOH, RT, 24 h, 30%; (iii) DCM, DIPEA, RT, 24 h, 59%; (iv) acetone, $NaHCO_3$, 0 °C for 15 min, and RT for 12 h, 25−53%.

Published in : Journal of Agricultural and Food Chemistryl (2024), vol. 72, n°37, pp. 20670-20678
DOI: 10.1021/acs.jafc.4c05094
Status : Postprint (Author's version)

Scheme 2. *Synthesis of Target Compounds 7a-z and 7aa-ai*[a]

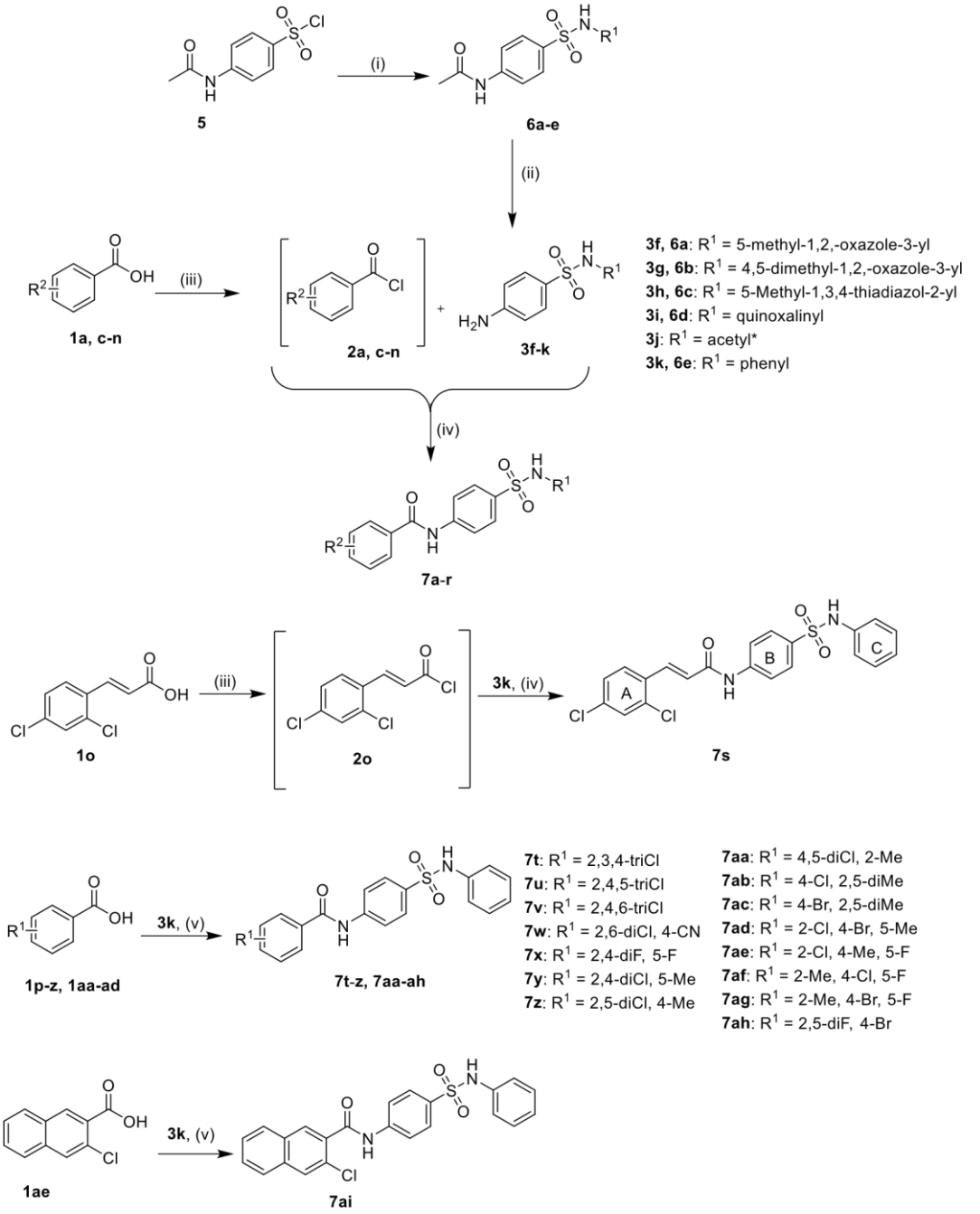

[a]Reagents and conditions: (i) amines, DCM, Et_3N, RT, 2 h, 62−78%; (ii) concentrated HCl, 100 °C, 2 h, 69−90%; (iii) DCM, $SOCl_2$, 50 °C, 1 h; (iv) acetone, $NaHCO_3$, RT, 12 h, 49−87%; (v) THF, T3P, pyridine, 60 °C, 12 h, 65−83%. *3j was commercially available. For substituents R^1 and R^2 for compounds 7a-r, please see Table 1.

Published in : Journal of Agricultural and Food Chemistryl (2024), vol. 72, n°37, pp. 20670-20678
DOI: 10.1021/acs.jafc.4c05094
Status : Postprint (Author's version)

PHARMACOLOGICAL EVALUATION OF COMPOUNDS (SERIES 1) ON GPR27V_2.

To estimate the SAR of the newly synthesized compounds (7a-z and 7aa-ai), we first resorted to a previously reported system that detects the recruitment of *β*-arrestin 2 to the activated receptor.[17,18] This complementation assay consists of a Firefly Luciferase (FLuc) split into two inactive parts. One moiety is attached to the N-terminal side of *β*arrestin 2 (*β*-Arr2-FLN). The other is fused to a chimeric version of GPR27 (GPR27V_2-LFC), where the C-terminal part of the receptor has been replaced with the one of the vasopressin V_2 receptors. This construct leads to a more sustained interaction with the arrestin and consequently to a more sensitive assay, which is a standard approach for characterizing GPCR ligands.[23]

SARS OF THE DISUBSTITUTED COMPOUNDS.

The disubstituted compounds 4a−e and 7a−e (see Table 1) were designed to investigate the role of ring C in the lead compound I. The elimination of ring C led to compounds 4a−e. The compound with sulfonic acid 4a resulted in a loss, while methylsulfonyl (4b, pEC_{50} 4.42) displayed reduced activity. Also, the sulfonamide derivatives 4c-e abolished the agonistic activity, suggesting the need for ring C for the agonistic activity.

In the next set of compounds, ring C was replaced with different heterocycles such as isoxazoles (7a, b), thiadiazole (7c), quinoxaline (7d), and acetyl (7e). However, none of the derivatives showed any agonistic activity, which reinforces the notion that the phenyl ring in the lead compound is critical for receptor activation.[18]

Since the previous study highlighted (i) the crucial role of the sulfonamide moiety (SO_2NH) between the aryl rings B and C and (ii) the significance of the amide moiety (CONH) between the rings A and B,[18] we next directed our attention to ring A (Table 1). First, 2,4-diCl replacements in the lead molecule I were substituted with various substituents, such as 2,4-diBr, 2,4-diCH_3, and 2,4-diCF_3. The rank order of potency for substituents in the 2,4-positions of ring A is as follows: >2,4-diCF_3 (7i, pEC_{50} 6.26) > 2,4-diCH_3 (7h, pEC_{50} 5.67) > 2,4-diBr (7f, pEC_{50} 5.49) ∼ 2,4-diF (7g, pEC_{50} 5.41). Compound 7i, in particular, had slightly improved agonistic activity compared to lead compound I (pEC_{50} ratio 1.10).

2-Cl was then held constant while 4-Cl was substituted with 4-CF_3, 4-OCH_3, and 4-CN. The resulting compounds containing 2-Cl,4-CF_3 (7j; pEC_{50} 5.41) and 2-Cl,4-CN (7l; pEC_{50} 5.23) demonstrated moderate activities, whereas 2-Cl,4OCH_3 (7k; pEC_{50} 5.09) significantly reduced the agonistic activity on GPR27V_2. When 4-Br was substituted with 4-OMe and 4-CF_3 in 7f, the agonistic activity of the resulting 2-Br,4OMe (7m: pEC_{50} 5.03) and 2-Br,4-CF_3 (7n: pEC_{50} 5.16) substituted derivatives was reduced. The GPR27 agonistic activity was abolished by the compound having 2-Me,4-OMe substitutions (7o: pEC_{50} N.D.).

Other combinations, such as 2-OMe,4-CF_3 (7p: pEC_{50} 5.91), 2-OCF_3,4-Cl (7q: pEC_{50} 6.71), and 2-OCH_3,4-Cl (7r: pEC_{50} 6.01), had a similar agonistic activity with a pEC_{50} ratio of ∼1 compared to that of the lead I. On the other hand, the compound 7s lost activity because it had an additional methylene unit between ring A and amide (CONH), suggesting that the direct connection of amide to ring A is also important for the activity.

Published in : Journal of Agricultural and Food Chemistryl (2024), vol. 72, n°37, pp. 20670-20678
DOI: 10.1021/acs.jafc.4c05094
Status : Postprint (Author's version)

In terms of efficacy (set at 100% for reference compound I), compounds such as 7i (E_{max}: 29%), 7j (E_{max}: 87%), and 7q (E_{max}: 54%) had significantly lower efficacies than the lead compound I, ranging from 29 to 87%. Compounds 7f (E_{max}: 108%), 7g (E_{max}: 98%), 7k (E_{max}: 94%), and 7p (E_{max}: 101%) Table 1. SARs of the First Series on GPR27V$_2$ had comparable efficacies to lead compound I. Agonists 7h (E_{max}: 144%), 7l (E_{max}: 122%), 7m (E_{max}: 126%), 7n (E_{max}: 163%), and 7r (E_{max}: 149%) demonstrated greater efficacies than the lead compound I. Concentration−response curves for the most interesting compounds (7h, 7m, 7n, 7p, and 7r), as well as for the lead compound I, are displayed in Figure 2.

Published in : Journal of Agricultural and Food Chemistryl (2024), vol. 72, n°37, pp. 20670-20678
DOI: 10.1021/acs.jafc.4c05094
Status : Postprint (Author's version)

Table 1. *SARs of the First Series on GPR27V₂*

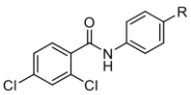
4a-b, 4e, 7a-e

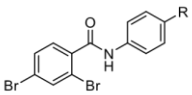
4c-d

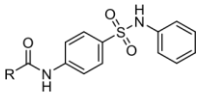
7f-s

Compounds	R	Human GPR27V₂		
		pEC₅₀[a] (I)[b]	E_{max} vs I (%)[c]	pEC₅₀ Ratio
I (8535)	For structure, see Figure 1.	6.38	100	
4a		<4	ND	ND
4b		4.42±0.14 (5.42±0.05)	166	0.88
4c		<4	ND	ND
4d		<4	ND	ND
4e		<4	ND	ND
7a		<4	ND	ND
7b		<4	ND	ND
7c	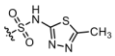	<4	ND	ND
7d	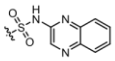	<4	ND	ND
7e		<4	ND	ND
7f		5.49 ± 0.07 (5.65 ± 0.10)	108	0.97
7g		5.41 ± 0.05 (5.65 ± 0.10)	98	0.96
7h		5.67 ± 0.17 (5.71 ± 0.19)	144	0.99
7i		6.26 ± 0.63 (5.73 ± 0.10)	29	1.10
7j		5.41 ± 0.14 (5.72 ± 0.08)	88	0.94
7k		5.09 ± 0.05 (5.44 ± 0.04)	94	0.93
7l		5.23 ± 0.06 (5.77 ± 0.11)	122	0.91
7m		5.03 ± 0.06 (5.73 ± 0.09)	126	0.88
7n		5.16 ± 0.07 (5.73 ± 0.09)	163	0.90
7o		<4	n.d.	n.d.
7p		5.91 ± 0.05 (5.77±0.11)	101	1.02
7q	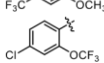	6.71 ± 0.78 (6.41 ± 0.21)	54	1.05
7r		6.01 ± 0.08 (6.04 ± 0.10)	149	0.99
7s		<4	ND	ND

[a]pEC_{50} values were measured in a *β*-arrestin 2 recruitment-based Firefly Luciferase complementation assay. Data points represent the mean ± SEM of three replicates. The activity of all compounds was verified in at least 2 independent experiments. [b]The pEC_{50} of the reference compound I is given in brackets for comparison with each tested compound. [c]E_{max} is expressed as the percentage of the maximal activity of the lead compound I. n.d. = not determined.

Published in : Journal of Agricultural and Food Chemistryl (2024), vol. 72, n°37, pp. 20670-20678
DOI: 10.1021/acs.jafc.4c05094
Status : Postprint (Author's version)

Figure 2. *Concentration−response curves for the most interesting compounds in the β-arrestin 2 recruitment assay. HEK293 cells stably transfected with the β-Arr2-FLN and GPR27V$_2$-LFC constructs. 7h (pEC$_{50}$ 5.67 ± 0.17, E$_{max}$ 144%), 7m (pEC$_{50}$ 5.03 ± 0.06, E$_{max}$ 126%), 7n (pEC$_{50}$ 5.16 ± 0.07, E$_{max}$ 163%), 7p (pEC$_{50}$ 5.91 ± 0.05, E$_{max}$ 101%), 7r (pEC$_{50}$ 6.01 ± 0.08, E$_{max}$ 149%). Data are mean ± SEM, representative of at least two independent experiments performed in triplicate.*

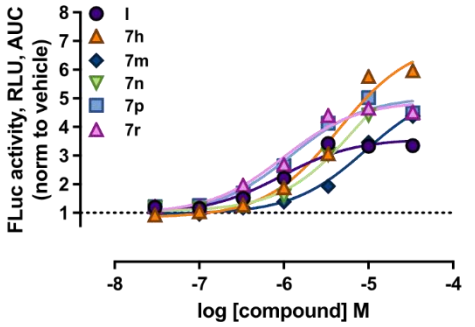

EVALUATION OF COMPOUNDS ON GPR27 WITHOUT THE V$_2$ TAIL.

The chimeric version of GPR27, GPR27V$_2$, has been used in our research program to facilitate the identification and development of active molecules and establish the pharmacophore for the agonistic activity of GPR27. However, we reasoned that this strategy could distort the efficacy of our compounds by promoting the establishment of more stable interactions between the activated receptor and *β*-arrestin 2. Therefore, we investigated the activities of the disubstituted compounds presenting the best profile on HEK293 cell lines stably expressing GPR27-LFC instead of GPR27V$_2$-LFC together with *β*-Arr2-FLN. Interestingly, while the potencies of the compounds were marginally affected, some efficacies were markedly improved compared to I, notably compound 7p (that we call PT-91, Figure 3).

Thus, we established 7p as the new reference agonist for GPR27 and compared the best disubstituted compounds to 7p to further improve our compounds (Table 2). The agonistic potencies of compounds 7f−h, 7l, 7n, and 7r were comparable to those of compound 7p. However, the efficacy of these compounds was much lower, except for 7r, which had better efficacy compared to 7p.

Published in : Journal of Agricultural and Food Chemistryl (2024), vol. 72, n°37, pp. 20670-20678
DOI: 10.1021/acs.jafc.4c05094
Status : Postprint (Author's version)

***Table 2**. Activities of Disubstituted Compounds on GPR27*

	human GPR27		
compounds	pEC_{50}[a] (7p)	E_{max} vs 7p (%)[b]	pEC_{50} ratio
I	5.62 ± 0.25	19	0.91
7p (PT-91)	6.15 ± 0.07	100	1.00
7f	5.91 ± 0.28 (6.44 ± 0.15)	10	0.92
7g	6.35 ± 0.24 (6.36 ± 0.13)	52	1.00
7h	6.11 ± 0.36 (5.90 ± 0.10)	30	1.03
7i	<4.5	n.d.	n.d.
7j	5.17 ± 0.94 (6.27 ± 0.21)	20	0.82
7k	<4.5	n.d.	n.d.
7l	6.01 ± 0.50 (6.41 ± 0.17)	30	0.93
7m	5.52 ± 0.47 (6.59 ± 0.19)	18	0.83
7n	6.61 ± 0.52 (6.34 ± 0.16)	13	1.04
7o	<4.5	n.d.	n.d.
7q	<4.5	n.d.	n.d.
7r	6.69 ± 0.17 (6.83 ± 0.53)	141	0.98

[a]pEC_{50} values were measured in a *β*-arrestin 2 recruitment-based firefly luciferase complementation assay. Data represent the mean ± SEM of three replicates. The active compounds were tested in at least 2 independent experiments. [b]E_{max} is expressed as the percentage of the maximal activity of 7p (PT-91) that was included in each test plate. n.d.not determined.

Molecular Docking Studies of 7p in the Orthosteric Pocket of the GPR27-*β*-Arrestin 2 Model.

Based on the agonistic activity at both wild-type GPR27 and $GPR27V_2$, the SAR is steep. In a nutshell, the agonistic activity was lowered or eliminated in lead chemical I for any ring C substitution, sulfonamide to amide conversion, or ring B change. In order to improve the activities of the first series, we docked our new reference compound 7p in a full-length GPR27 homology model bound with *β*-arrestin 2 generated from the structure of rhodopsin bound to visual arrestin.[24]

Figure 3.

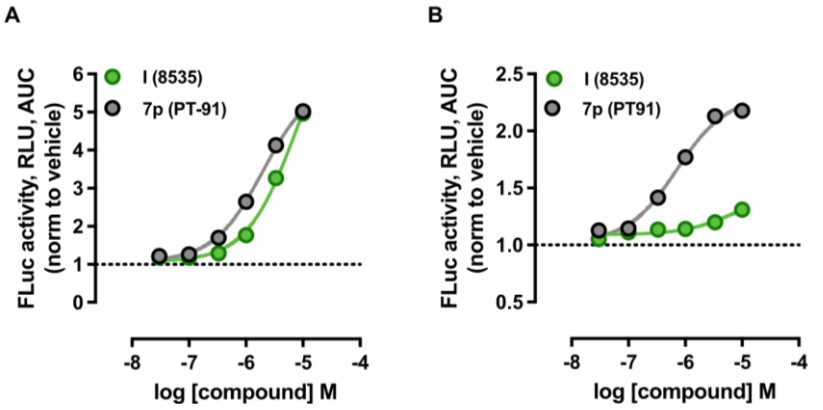

Concentration−response curves for compound 7p (PT-91) and reference agonist I (8535) in the *β*-arrestin 2 recruitment assay. The experiments were done on HEK293 cells stably transfected with *β*-Arr2-FLN and either $GPR27V_2$-LFC (A) or GPR27-LFC (B) constructs. (A) 7p (pEC_{50} 5.70 ± 0.06, E_{max} 462 ± 48%), I (5.13 ± 0.07, E_{max} 100%). (B) 7p (pEC_{50} 6.15 ± 0.07, E_{max} 112 ± 5%), I (5.18 ± 0.39, E_{max} 100%). Data are mean ± SEM, representative of at least four independent experiments performed in triplicate.

Published in : Journal of Agricultural and Food Chemistryl (2024), vol. 72, n°37, pp. 20670-20678
DOI: 10.1021/acs.jafc.4c05094
Status : Postprint (Author's version)

Figure 4.

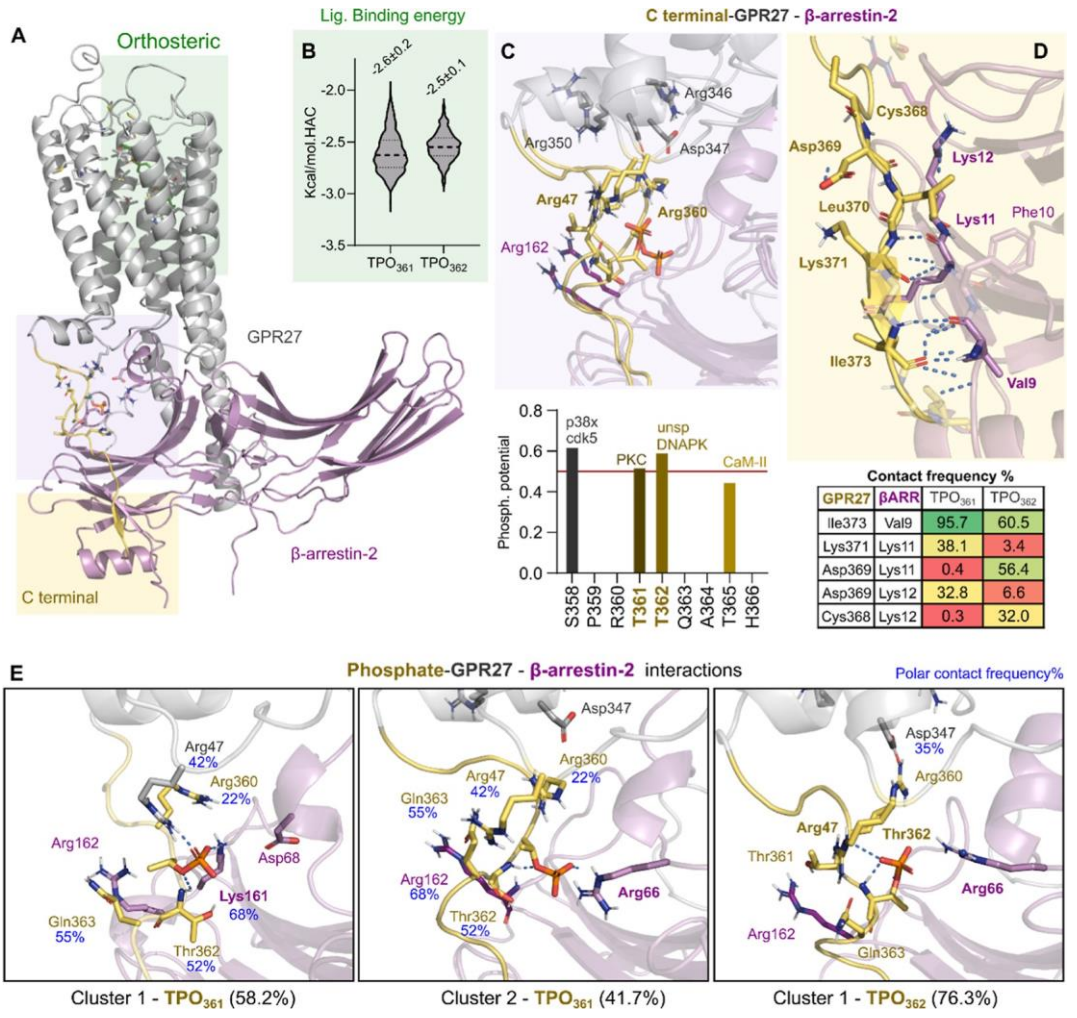

Overview of the GPR27 full model with *β*-arrestin 2 highlighting its C-terminal interaction and phosphorylation sites (PDB ID: 5W0P). (A) GPR27 (gray) with *β*-arrestin 2 (purple) full model highlighting the C-terminal interaction and phosphorylation sites (yellow). (B) Freebinding energy (calculated by MM/GBSA and normalized by the number of heavy atoms, HAC) for compound 7p calculated for both alternative phosphorylation models, showing that the phosphorylation state has little effect on the orthosteric binding energy on simulations. (C) Upper, representative frame of the C-terminal phosphorylation sites Thr361 and Thr362 and, bottom, their respective prediction scores (0−1.0 where >0.5 means likely to be phosphorylated by the labeled kinase). (D) Upon simulation, the C-terminal tail stabilizes a complementary strand to the *β*arrestin 2 beta-sheets supported by the interactions depicted in the upper panel and quantified in the bottom table (contact frequency % and expanded in Table S1). (E) Representative frame from the 7p simulations in GPR27 depicting the most common interactions around the phosphate residues. The frequency of interaction with depicted amino acids along the analyzed trajectory (5 μs) is shown in blue (polar interactions) and quantified in Table S1.

Published in : Journal of Agricultural and Food Chemistryl (2024), vol. 72, n°37, pp. 20670-20678
DOI: 10.1021/acs.jafc.4c05094
Status : Postprint (Author's version)

The final model was composed of seven transmembrane (TM) helices, the eighth helix in parallel with the membrane, and an intracellular region (Figure 4A). GPR27's TM5 has a further extension toward the intracellular space, which, together with the C-terminal extension, is responsible for the interaction with β-arrestin 2. During the execution of this project, there was no template covering the C-terminal region (residues 356−371), which was bent toward the cytoplasm and anchored between the two β-sheet clusters of β-arrestin 2, according to the rhodopsin-bound structure (PDB ID: 5W0P[24]). Following the predictions of potential phosphorylation sites, we generated GPR27-Thr361(P_i)-β-arrestin 2 (herein named as GPR27-TPO_{361}) and GPR27-Thr362(P_i)-βarrestin 2 (herein GPR27-TPO_{362}) models, which were employed for further studies.

Herein, we chose to use a flexible docking approach followed by molecular dynamics (MD) simulations to validate this pose as an alternative manner to account for the receptor flexibility.

Altogether, we have simulated ∼10 μs simulations for compound 7p split between both phosphorylated models TPO_{361} and TPO_{362}. Both models display comparably lower overall binding energy (Figure 4B). The added phosphate groups are consistent with predicted phosphorylation sites and are geometrically sandwiched by a pair of arginine side-chains each (Figure 4C,E). The C-terminal peptide was predicted to generate a beta-strand, which would pair with the *β*-arrestin strands (Figure 4D), establishing stable backbone−backbone contacts between the Val9 (*β*-arrestin) and Ile373 (GPR27) during the MD simulations (Figure 4D, Table) for GRP27TPO361, which further supports the relevance of this phosphorylation site.

Comparison between the proposed binding models of 7p with either GPR27-TPO_{361} or GPR27-TPO_{362} (Tables S1 and S2) shows that 7p engages in stabler interactions with a higher interaction frequency in the GPR27-TPO_{361} model, which was therefore further discussed. The potential binding mode of 7p (Figure 5) suggests stable hydrogen bond interactions between its sulfonamide group and the backbone from Pro170 (∼95% of the analyzed trajectory) and a transient water-mediated interaction with the side chain of Tyr325 (∼40%), while the amide group stably interacts with Leu173's backbone (89%). 2-OMe, 4-CF_3-substituted aryl ring of 7p, displays hydrophobic contacts with Cys106, Trp297, and Tyr300 side chains. We predicted that around ring A of 7p, there was some space (Figure 5B,C) that could accommodate additional substituents, preferably hydrophobic ones. We reasoned that trisubstituted compounds would fill the pocket more tightly and lead to agonists with improved affinity and activity.

Published in : Journal of Agricultural and Food Chemistryl (2024), vol. 72, n°37, pp. 20670-20678
DOI: 10.1021/acs.jafc.4c05094
Status : Postprint (Author's version)

Figure 5.

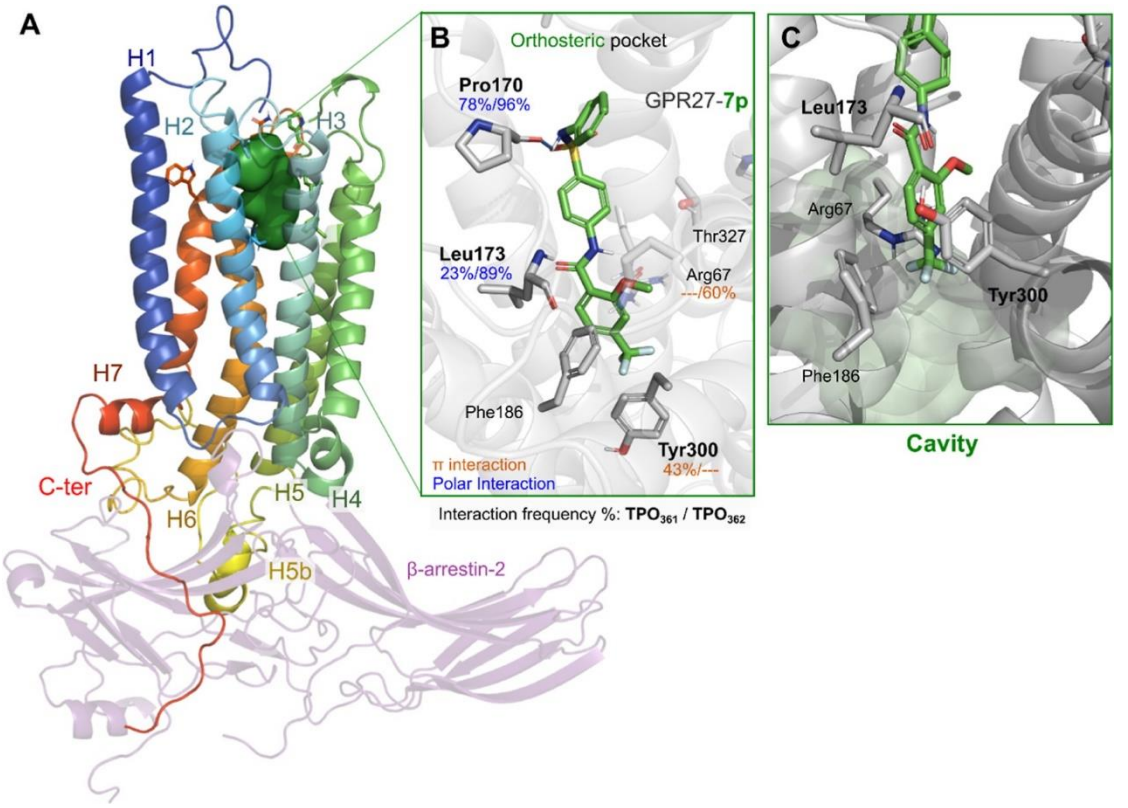

(A) Overview of the GPR27 model highlighting the different helices and the binding site as a surface. (B) Docking studies of 7p into the GPR27-*β*-arrestin 2 model. Representative frame from the 7p simulation in the GPR27 putative binding site. The frequency of interaction with depicted amino acids along the analyzed trajectory (5 μs) is shown in blue (polar interactions) or orange (π contacts). (C) Surface representation of the bottom of the binding cavity.

EVALUATION OF TRISUBSTITUTED COMPOUNDS ON GPR27.

Following our docking investigations, we designed and synthesized the trisubstituted compounds 7t-z and 7aa-ai (Scheme 2) and evaluated their agonistic activity on GPR27 (Table 3). In general, the trisubstituted compounds were characterized by improved potencies compared to the disubstituted ones.

The compounds with 2,3,4-triCl (7t) and 2,4,5-triCl (7u) substituents had a similar potency compared to 7p but were better than the corresponding disubstituted ones, i.e., compound I. On the other hand, the introduction of the substituent at position 6 on ring A reduced the potency (see compounds 7v and 7w). The insertion of 5-F in I that leads to 7x maintained the potency observed for I but with a slightly reduced potency compared to 7p. Other combinations like 2,4diF,5-Me (7y), 2,5-diCl,4-Me (7z), 4,5-diCl, 2-Me (7aa), 4Cl,2,5-diMe (7ab), 4-Br,2,5-diMe (7ac), and 4-Br,2-F,5-Me (7ad) maintained or slightly increased the agonistic activity compared to the new lead 7p. Compounds 7ab and 7ac, in particular, had a better profile, with pEC_{50} values of 6.56 (pEC_{50} ratio of 1.05) and 6.90 (pEC_{50} ratio of 1.12). Compound 7ae with 2-Cl,4-Me,5-F, however, had a reduced potency. Further derivatives such as 7af (pEC_{50} 6.09; ratio 0.97),

Published in : Journal of Agricultural and Food Chemistryl (2024), vol. 72, n°37, pp. 20670-20678
DOI: 10.1021/acs.jafc.4c05094
Status : Postprint (Author's version)

7ag (pEC_{50} 6.25; ratio 1.0), 7ah (pEC_{50} 6.38; ratio 1.02), and the bicyclic compound 7ai (pEC_{50} 6.02; ratio 1.02) displayed a similar agonistic profile compared to 7p.

The efficacies were compared to the one of 7p on GPR27, which was set at 100%. As shown in Table 3, compounds such as 7y (E_{max}: 95%), 7aa (E_{max}: 89%), 7ab (E_{max}: 99%), 7ac (E_{max}: 88%), 7af (E_{max}: 99%), and 7ag (E_{max}: 99%) displayed efficacies like 7p, indicating their full agonist profile regarding the reference. Compounds 7z (E_{max}: 45%), 7ad (E_{max}: 40%), 7ah (E_{max}: 60%), and 7ai (E_{max}: 46%) showed moderate efficacies, ranging from 40 to 60%, suggesting partial agonism regarding 7p. The availability of active ligands with various efficacies should aid in determining the receptor's physiological relevance. The other compounds showed significantly lower efficacies. The concentration−response curves for the best compounds (7ab and 7af) are illustrated in Figure 6.

Molecular Docking Studies of 7v in the GPR27-β-arrestin 2 Model.

The compound 7ab displays improved potency compared to 7p. Thus, we performed docking of 7ab in our GPR27-*β*-arrestin 2 model. Interestingly, in our simulation, the 4-Cl, 2,5-diMe-substituted aryl ring of 7ab did reach the deeper part of the orthosteric pocket (Figure 7), establishing hydrophobic contacts with Tyr300 (during 30−37% of the analyzed simulation time) and Phe186 (27%). Its sulfonamide group stably interacts with the Leu173's backbone (∼94%) and to some extent with Cys95 (∼25%), locking it on the surface of the pocket. Our previous work[18] suggested, based on a combination of docking and WaterMap studies, that the orthosteric pocket's bottom harbors high-energy hydration sites, which could contribute to the binding energy when occupied by hydrophobic moieties. Here, we establish the relevance of trisubstituted aryl rings, in comparison with the double substituted ones, in occupying this deeper pocket since the compounds with longer interaction time were also more active.

Published in : Journal of Agricultural and Food Chemistryl (2024), vol. 72, n°37, pp. 20670-20678
DOI: 10.1021/acs.jafc.4c05094
Status : Postprint (Author's version)

Table 3. *Activity of Trisubstituted Compounds on GPR27*

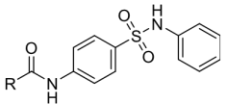

7t-z, 7aa-ai

Compounds	R	Human GPR27		
		pEC$_{50}$[a] (**7p**)	E$_{max}$ vs **7p** (%)[b]	pEC$_{50}$ Ratio
7t	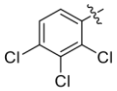	6.20 ± 0.42 (6.19 ± 0.10)	29	1.00
7u	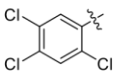	6.23 ± 0.09 (6.46 ± 0.21)	93	0.96
7v	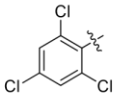	<4.5	n.d.	n.d.
7w	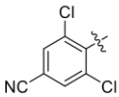	<4.5	n.d.	n.d.
7x	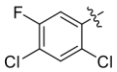	6.42 ± 0.65 (6.46 ± 0.21)	15	0.99
7y	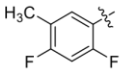	6.43 ± 0.26 (6.57 ± 0.43)	95	0.98
7z	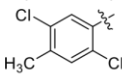	6.44 ± 0.23 (5.90 ± 0.10)	45	1.09
7aa	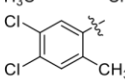	6.58 ± 0.36 (6.28 ± 0.17)	89	1.04
7ab	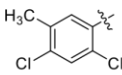	6.56 ± 0.28 (6.20 ± 0.28)	99	1.05
7ac	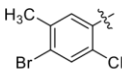	6.90 ± 0.30 (6.13 ± 0.18)	88	1.12
7ad	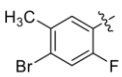	5.67 ± 0.21 (6.46 ± 0.17)	40	0.88
7ae	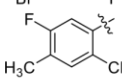	<4.5	n.d.	n.d.
7af	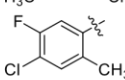	6.09 ± 0.15 (6.25 ± 0.14)	99	0.97
7ag	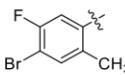	6.25 ± 0.20 (6.25 ± 0.14)	85	1.00
7ah	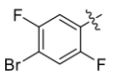	6.38 ± 0.24 (6.25 ± 0.14)	60	1.02
7ai	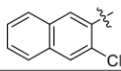	6.02 ± 0.22 (5.90 ± 0.10)	46	1.02

[a]pEC$_{50}$ values were measured in a *β*-arrestin 2 recruitment-based firefly luciferase complementation assay. Data represent the mean ± SEM of three replicates. The active compounds were tested in at least 2 independent experiments. [b]E_{max} is expressed as the percentage of the maximal activity of 7p (PT-91) that was included in each test plate. n.d.not determined.

Published in : Journal of Agricultural and Food Chemistryl (2024), vol. 72, n°37, pp. 20670-20678
DOI: 10.1021/acs.jafc.4c05094
Status : Postprint (Author's version)

Figure 6. *Concentration–response curves for selected trisubstituted compounds (7ab and 7af) in the GPR27-β-arrestin 2 recruitment assay. Lead compound 7p and reference compound I are included for comparison. The experiments were done on HEK293 cells stably transfected with the β-Arr2-FLN and GPR27-LFC constructs. 7p (pEC_{50} 6.34 ± 0.15, E_{max} 100 ± 8%), I (5.62 ± 0.25, E_{max} 23 ± 3%), 7ab (pEC_{50} 6.70 ± 0.22, E_{max} 90 ± 11%), 7af (6.73 ± 0.21, E_{max} 57 ± 7%). Data are mean ± SEM, representative of at least two independent experiments performed in triplicate.*

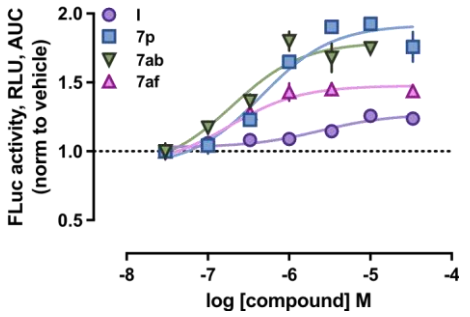

Figure 7. *Proposed binding mode for an example of trisubstituted compound. (A) Potential binding mode of the trisubstituted compound 7ab. The frequency of interaction with depicted amino acids along the analyzed trajectory (5 μs) is shown in blue (polar interactions) or orange (π-contacts).*

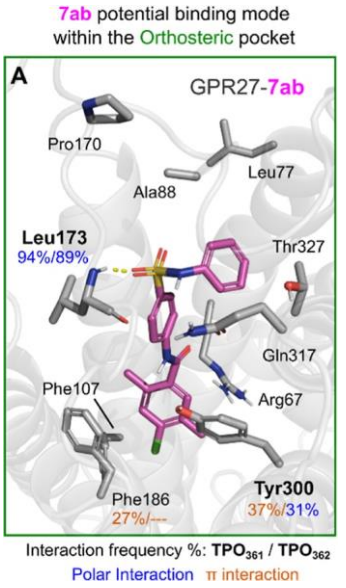

DETERMINATION OF NEW GPR27 AGONISTS' SPECIFICITY AND SELECTIVITY.

In order to confirm the selective activation of GPR27 with our newly synthesized compounds, we designed and generated a complementation assay for the adrenoceptor β_2 (β_2AR) based on the same principles. We evaluated the response of compounds 7p, 7r, 7ab, and 7af on a HEK293 cell line stably expressing β-Arr2-FLN and β_2AR-LFC. We added isoproterenol, a potent β_2AR agonist, as a control for

Published in : Journal of Agricultural and Food Chemistryl (2024), vol. 72, n°37, pp. 20670-20678
DOI: 10.1021/acs.jafc.4c05094
Status : Postprint (Author's version)

receptor activation. Our data show an absence of measurable β_2AR activation by our compounds in this control assay (Figure 8).

Figure 8. *Concentration−response curves for selected compounds (7p, 7r, 7ab, and 7af) in the β_2AR-β-arrestin 2 recruitment assay. Reference agonist isoproterenol is included as a positive control. The experiments were done on HEK293 cells stably transfected with the β-Arr2-FLN and β_2AR-LFC constructs. Isoproterenol (pEC_{50} 6.83 ± 0.03, E_{max} 100 ± 2%). Data are mean ± SEM, representative of one experiment performed in triplicate.*

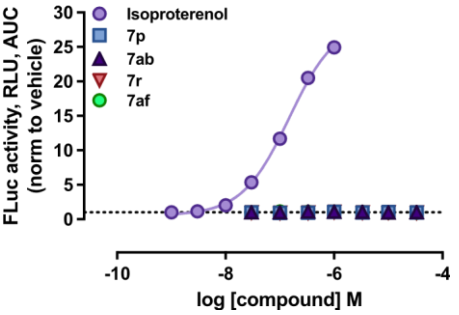

G Protein Activation by GPR27.

An important question that remains unanswered is the ability of GPR27 to activate G proteins. It has been increasingly observed that some GPCRs cannot couple to G proteins and are labeled as "atypical" or "intrinsically biased toward β-arrestins".[25,26] Following the identification of I with a β-arrestin 2 complementation assay, we failed to observe any activity in the G-protein-based assay.[17] Several hypotheses were proposed to explain this observation. Besides the possibility that GPR27 is an atypical, non-G protein-coupled receptor, it is also conceivable that the efficacy of I was rather weak, and the G-protein assays were inadequately sensitive in that context. Therefore, having identified novel compounds with a marked increase of efficacy compared with I, on the receptor without the V_2 tail (Figure 3), we sought to verify the activity of 7p on GPR27 in assays measuring G protein activation. We started with two different tests on different cell types to measure the levels of intracellular cAMP that reflect coupling to G_s- or $G_{i/o}$-protein families. The first assay is an end point measurement of cAMP accumulation after 30 min stimulation with the compounds[27] (Figure 9A), while the other is a kinetic measurement based on the cAMP Glo sensor technology in live cells[28] (Figure 9B). These experiments revealed that 7p, 7ab, or 7af did not significantly influence the levels of cAMP through GPR27 (Figure 9A,B).

Next, we tested the capacity of 7p to induce the dissociation of different G proteins with a newly described assay[29] that monitors bioluminescence resonance energy transfer (BRET) signal between G_α and G_γ subunits. In this system, 7p did not induce G_{i1}, G_q, or G_{12} protein dissociation when GPR27 was present (Figure 10A−C).

These data are in line with our previous observations on the apparent absence of GPR27-induced G protein activation. Interestingly, Jang et al. (2023) recently reported that all three

Published in : Journal of Agricultural and Food Chemistryl (2024), vol. 72, n°37, pp. 20670-20678
DOI: 10.1021/acs.jafc.4c05094
Status : Postprint (Author's version)

SREBs (GPR27, GPR85, and GPR173) were devoid of G protein association using an elegant approach based on nucleotide-decoupled G protein variants able to bind spontaneously to a GPCR in its inactive conformation.[26] The question of the atypicality of GPR27 requires a thorough pharmacological investigation that is outside of the scope of the present report.

Metabolic Stability, Cytotoxicity, and In Vivo PK Study.

For further profiling, the molecule 7p was selected. First, the potential cytotoxicity of 7p was evaluated in HEK 293 (along with the other representative compound 7af) using the cell- titer glo assay. Different concentrations of the compound were examined and did not show significant impact on general cell viability (Figure S1). The metabolic stability of the new lead 7p was studied in human liver microsomes (HLM) (Figure 11) and mouse liver microsomes (MLM) (Figure 11). A negative and positive control against 7p was tested to avoid errors due to fluctuations in the metabolism of the microsomes. In general, the compound was very stable in both HLM and MLM, retaining more than 60% (HLM: 79.9%, MLM: 64.7%) even after 120 min (Table S4).

To estimate the oral absorption and brain exposure, we administered 7p intravenously at a dose of (1 mg/kg i.v.) and orally (10 mg/kg p.o.) (n = 3 animals) (see Figure 11b). Under i.v. (1 mg) application, a C_{max} of 2933 was achieved with an approximate $t_{1/2}$ of 180 min. Oral administration (10 mg) yielded a C_{max} of 8149 with an approximate $t_{1/2}$ of 160 min. The approximate bioavailability (F) via the oral route was 59%, which is indicative of adequate overall properties and a robust formulation effect.

Organ concentrations were also calculated using an approximate assumption of 1 mg tissue = 1 μL fluid (Table 4). On this basis, nM approximates to nmol/kg, which is convenient for relating in vitro inhibition data to in vivo levels. The whole brain concentration of 7p at 240 min (i.v.) was 163 nM (34% of heart plasma) and the level at 480 min (p.o.) was 164 nM (39% of heart plasma). These data suggest that brain exposure was related to overall plasma concentration and reaches 25−40% of peripheral (tail) and central (heart) plasma concentrations, respectively. This, in turn, suggests that there is probably a rapid equilibrium between brain and plasma. The tissue and blood levels were above the EC_{50} for the main target GPR27, suggesting that 7p can be used as a new tool compound for future studies on the pharmacology of the native GPR27.

Published in : Journal of Agricultural and Food Chemistryl (2024), vol. 72, n°37, pp. 20670-20678
DOI: 10.1021/acs.jafc.4c05094
Status : Postprint (Author's version)

Figure 9. *Determination of the impact of 7p, 7ab, and 7af on cAMP levels by two different methods. (A) End point measurement (ALPHAscreen technology) of HEK293 cells transiently transfected with GPR27 or an empty vector (EV) and stimulated for 30 min with the indicated compounds. (B) Kinetic measurement of cAMP levels on HEK293 cells stably transfected with GPR27 and pGlo sensor. Cells were stimulated for 10 min by the indicated compounds before addition of FLuc substrate and recording in the plate luminometer for 30 min. Data are mean ± SEM of (A) three independent experiments and (B) one representative of at least two independent experiments performed in triplicate.*

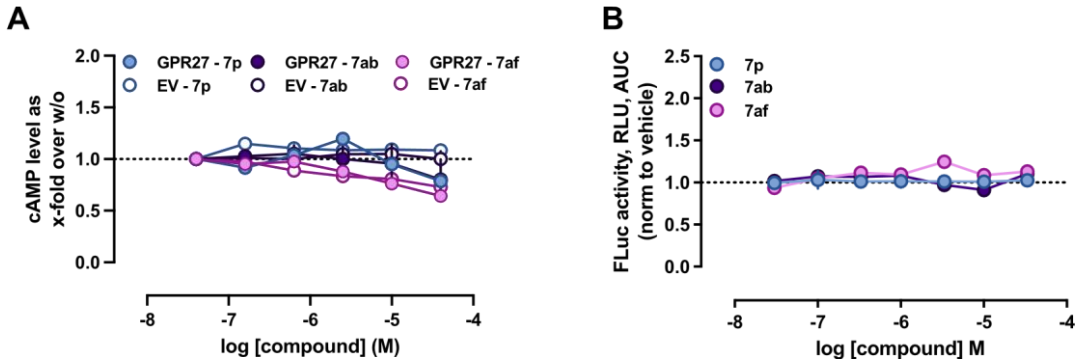

Figure 10. *Determination of G protein activation by GPR27 upon treatment with 7p. HEK293 cells were transiently transfected with BRET-based G protein sensors combined on a single plasmid (G-CASE) expressing Gβ, Gγ fused with an acceptor (circularly permutated Venus), and Gα fused with the donor, nanoluciferase (NLuc) together with GPR27 (7p) or (A) histamine receptor H_3 for G_{i1}-CASE (histamine pEC_{50} 7.71 ± 0.14). (B) Muscarinic receptor M_3 for G_q-CASE (carbachol pEC_{50} 7.07 ± 0.24). (C) Thromboxane receptor TP for G_{13}-CASE (U46619 pEC_{50} 8.13 ± 0.05). Cells were incubated with NLuc substrate for 5 min, mixed with the compounds and further incubated for 10 min. Emission was recorded at 450 and 535 nm to determine the raw BRET ratio (Em_{535}/Em_{450}). Shown are the raw BRET ratios normalized to the vehicle. Data are mean ± SEM, representative of at least two experiments performed in triplicate.*

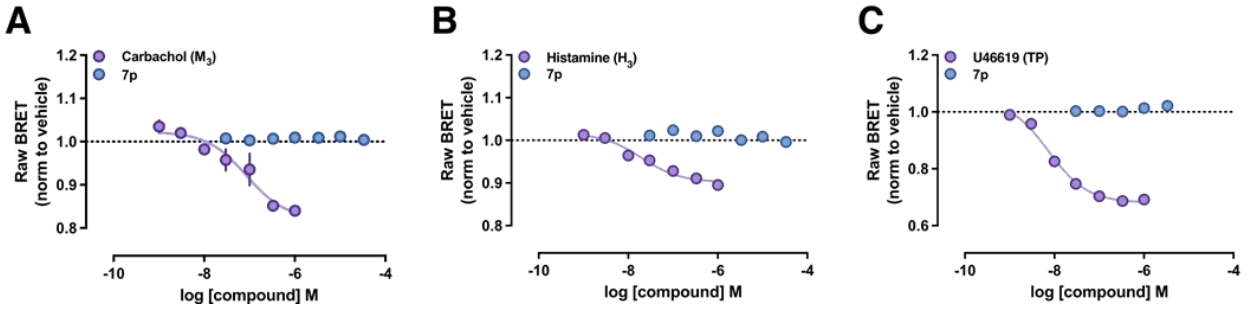

Published in : Journal of Agricultural and Food Chemistryl (2024), vol. 72, n°37, pp. 20670-20678
DOI: 10.1021/acs.jafc.4c05094
Status : Postprint (Author's version)

Figure 11. *(A) In vitro metabolism of compound 7p in human liver microsomes (squares) and mouse liver microsomes (circles) (20 mg/mL, male, pooled). Compounds were tested at a concentration of 100 μM. Data are the mean ± SD (for details, see the Experimental Section). (B) Plasma levels of 7p in C57B6 female mice following application of 1 mg/kg i.v. or 10 mg/kg p.o. (n = 3).*

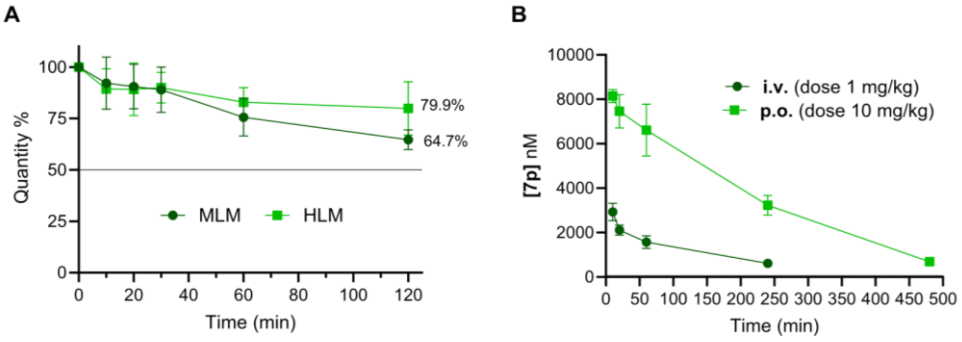

Table 4. *Tissue Levels of 7p (in nM or nmol/kg) at 4 h Post 1 mg/kg i.v. or Application or 8 h Post 10 mg/kg p.o.*[a]

route-dose	i.v.-1 mg/kg		p.o.-10 mg/kg	
time	240 min		480 min	
	mean	confidence	mean	confidence
heart plasma	475	60	417	41
liver	649	16	536	49
spleen	260	34	301	8
brain	163	17	164	3

[a]Data are the mean of *N* = 3 animals and are presented with a 95% confidence interval.

Conclusions

In conclusion, we designed and synthesized a series of 40 novel di- and trisubstituted benzamide derivatives (7a-z and 7aa−ai) and evaluated them to optimize their GPR27 activity in an *β*arrestin 2 recruitment-based assay. The findings generally showed very steep SARs. The disubstituted benzamide derivatives 7a−s were first tested on the chimeric GPR27V_2 receptor. This first series of experiments revealed several interesting compounds, including 7f, 7h, 7l, 7m, 7n, 7p, and 7r, which had similar potencies and efficacies compared to the lead compound I. The potencies of the compounds were marginally impacted when evaluated on the native receptor GPR27 without the V_2 tail; however, several efficacies were noticeably better than the ones of I, most notably compound 7p. Second, to increase the GPR27 agonistic activity, we employed docking to design the subsequent tri- or bicyclic benzamide derivatives 7t-z and 7aa-ai based on 7p. With full agonistic activity, compounds 7u, 7y, 7ab, 7ac, and 7af were found to be among the best. The representative compounds 7p, 7r, 7ab, and 7af confirmed the

Published in : Journal of Agricultural and Food Chemistryl (2024), vol. 72, n°37, pp. 20670-20678
DOI: 10.1021/acs.jafc.4c05094
Status : Postprint (Author's version)

selective activation of GPR27 over the control receptor β_2AR. It is important to note that the selectivity of our compounds series has been evaluated only on the β_2AR. Although this gives a good indication of the specificity of our compounds toward GPR27, a thorough screening on representative members of the whole GPCRome would be necessary to use these chemical probes in more physiologically relevant or complex models. These aspects will be investigated in the near future and are beyond the scope of the present study.

The additional evaluations with these novel tools reinforce the notion that GPR27 is an atypical, β-arrestin-biased receptor unable to couple to G proteins. This observation further corroborates our previous and other teams reports, although the true pharmacological properties of GPR27 remain elusive. Additionally, the novel tool agonist 7p, at concentrations compatible with receptor activation, did not show cytotoxicity, was metabolically stable, and had good in vivo pharmacokinetic properties. Thus, we have significantly improved the available toolbox to investigate the complex function of GPR27 and provided new evidence of its atypical profile.

Experimental section

GENERAL EXPERIMENTAL PROCEDURES FOR CHEMICAL SYNTHESIS.

All commercially available reagents and solvents were used as received. Reactions sensitive to air or moisture were performed under an atmosphere of argon and/or in anhydrous solvents. Anhydrous solvents were purchased from Acros Organics (AcroSeal). Unless stated otherwise, extracts were dried over sodium sulfate prior to filtration. Thin-layer chromatography was performed on TLC Silica Gel 60 F254 aluminum sheets provided by Merck, with detection at 254 and 366 nm. Flash chromatography was carried out on an Interchim PuriFlash XS420 flash chromatography system and Grace Davison Davisil LC60A 20 × 10^{45} mm silica or Merck Geduran Si60 63-200 μm. Mass spectra were recorded on an Advion DCMS interface (ESI voltage: 3.50 kV, capillary voltage: 187 V, source voltage: 44 V, capillary temperature: 250 °C, desolvation gas temperature: 250 °C, gas flow rate: 5 L/min N_2), with elution of the spots with MeOH. High-resolution mass spectrometry (HRMS) for the final compound was measured by the mass spectrometry department, Institute of Organic Chemistry, Eberhard Karls University Tuebingen, on a Bruker maXis 4G ESI-TOF instrument. The instrument was run in ESI + mode, and the settings were as follows: nebulizer gas of 1.2 bar, gas flow of 6.0 L/min, source temperature of 200 °C, capillary voltage of 4500 V, end plate offset of −500 V, and *m*/*z* range from *m*/*z* 80 to 1000. NMR spectra were measured on Bruker Avance 400 or 600 NMR spectrometers. The spectra were calibrated on the deuterated solvents and chemical shifts (d) are stated relative to tetramethylsilane in ppm. The solvents used were deuterated chloroform (d_3) and deuterated DMSO (d_6). Melting points were measured on a melting point apparatus (Mettler Toledo MP70, hand method, temperature from 60 to 250 °C, heating rate 20.0 °C/min) and are uncorrected.

Published in : Journal of Agricultural and Food Chemistryl (2024), vol. 72, n°37, pp. 20670-20678
DOI: 10.1021/acs.jafc.4c05094
Status : Postprint (Author's version)

The purity of the final compound was determined via HPLC using an Agilent 1100 Series LC system (Agilent Technologies, Santa Clara, CA) with a Phenomenex Kinetex C8 100A column (150 mm × 4.6 mm, 2.6 μm) (Phenomenex Inc., Torrance, CA), and detection was performed with a UV DAD at the wavelength of 254 nm. Elution was carried out with the following gradients: 0.01 M KH_2PO_4 (pH 2.32) (solvent A) and MeOH (solvent B). Method A: 0 min, 40% B/60% A; 9 min, 95% B/5% A; 10 min, 95% B/5% A; 11 min, 40% B/60% A; 16 min, 40% B/60% A; the flow of 0.5 mL/min. Method B: 0 min, 40% B/60% A; 15 min, 85% B/15% A; 20 min, 85% B/15% A; 22 min, 40% B/60% A; 28 min, 40% B/60% A; flow 0.5 mL/min. The final compounds showed a purity of >95% according to the peak areas.

General Procedure for the Synthesis of Carboxylic Acid Chlorides (2a, b).

Dimethylformamide and thionyl chloride (1.0 mL) were added dropwise, one at a time, to a solution of carboxylic acid (1a or 1b, 5.0 mmol) in dichloromethane (30 mL). The mixture was concentrated under vacuum, and dichloromethane (4× 10 mL) was added to eliminate extra thionyl chloride after the reaction had finished, as determined by TLC.

Synthesis of 4-(2,4-Dichlorobenzamido)benzenesulfonic Acid (4a).

The carboxylic acid chloride (2a, 5.0 mmol) was subjected to a treatment with sulfanilic acid (3a, 5.1 mmol) in 5% sodium hydroxide (2 mL). The reaction mixture was stirred vigorously overnight at room temperature. The resulting product 4a was acidified in aqueous HCl (6 N, 5 mL) until a pH of 5 was established. The mixture was washed with small portions of ice-cold water (3× 20 mL), and the water solution was evaporated under reduced pressure to dryness. Yield: 59% (30 mg). mp 181−183 °C. ^{1}H NMR (500 MHz, DMSO-d_6): δ 10.56 (s, 1H), 7.74 (d, J = 2.0 Hz, 1H), 7.63− 7.61 (m, 3H), 7.56 (d, J = 8.6 Hz, 2H), 7.55−7.51 (m, 1H). ^{13}C NMR (126 MHz, DMSO-d_6): δ 164.17, 144.26, 138.86, 135.88, 135.00, 132.51, 131.41, 130.54, 130.36, 129.33, 127.68, 127.60, 127.19, 126.35, 118.75. HRMS (ESI-TOF) m/z: for ($C_{13}H_{10}Cl_2NO_4S$ $[M + H]^+$) calcd, 345.9708; found, 345.9702. HPLC t_R = 6.46 min.

Synthesis of 2,4-Dichloro-N-(4-(methylsulfonyl)phenyl)benzamide (4b).

To the solution of 2,4-dichlorobenzoyl chloride (2a, 5.0 mmol) in dichloromethane (10 mL), 4-(methylsulfonyl)aniline (3b, 5.1 mmol, 1.1 equiv) was added slowly at 0 °C. After stirring for 1 min, DIPEA (0.230 mL, 14.5 mmol, 2.5 equiv) was slowly added, drop by drop. TLC monitored the reaction's progress. After the reaction was completed, iced water was added, and the aqueous layer was extracted with dichloromethane. 2 N HCl was added to the organic layer to remove DIPEA. The collected organic layer was dried over magnesium sulfate, and the organic solvent was concentrated under vacuum. The residue was washed with dichloromethane twice to produce a pure compound. Yield: 59% (101 mg). mp 161−163 °C. ^{1}H NMR (600 MHz, DMSO-d_6): δ (ppm) 10.97 (s, 1H), 8.05−8.02 (m, 2H), 8.01−7.88 (m, 2H), 7.79 (d, J = 8.0 Hz, 1H), 7.67 (d, J = 8.2 Hz, 1H), 7.58 (dd, J = 8.2, 2.0 Hz, 1H), 3.17 (s, 3H). ^{13}C NMR (151 MHz, DMSO): δ (ppm) 143.27, 135.66, 135.40, 135.40, 135.33, 131.39, 130.56, 129.45, 128.44, 127.71, 119.63, 43.98. HRMS (ESI-TOF) m/z: for ($C_{14}H_{12}Cl_2NO_3S$ $[M + H]^+$) calcd, 343.9915; found, 343.9914. HPLC t_R = 7.53 min.

Published in : Journal of Agricultural and Food Chemistryl (2024), vol. 72, n°37, pp. 20670-20678
DOI: 10.1021/acs.jafc.4c05094
Status : Postprint (Author's version)

General Procedure for the Synthesis of 4c-e.

To the solution of appropriate carboxylic acid chloride (2a or 2b, 5.0 mmol) in acetone (20 mL), sulfanilamide derivatives (3c-e, 5.5 mmol) and sodium bicarbonate (20 mmol) were added. TLC monitored reaction progress. After the reaction was completed, the solvent was evaporated under vacuum. The reaction mixture was washed with ice-cold water (3× 30 mL) and filtered.

2,4-Dibromo-N-(4-sulfamoylphenyl)benzamide (4c).

This product was synthesized using 2,4-dibromo benzoic acid (1b, 140 mg, 5 mmol) via its carboxylic acid chloride (2b) and 4-aminobenzenesulfonamide (3c, 95 mg, 5.5 mmol) in the presence of $NaHCO_3$ (172 mg, 20 mmol). Colorless solid. Yield: 34% (75 mg). mp: 231−233 °C. ^{1}H NMR (600 MHz, DMSO-d_6): δ (ppm) 10.86 (s, 1H), 8.01 (d, J = 1.9 Hz, 1H), 7.85−7.82 (m, 2H), 7.82−7.78 (m, 2H), 7.74−7.71 (m, 1H), 7.68 (s, 1H), 7.55 (d, J = 8.1 Hz, 1H), 7.27 (s, 2H). ^{13}C NMR (151 MHz, DMSO-d_6): δ (ppm) 166.77, 165.59, 141.74, 139.29, 137.97, 135.92, 134.87, 132.35, 130.98, 130.62, 126.91, 123.62, 120.31, 119.40. HRMS (ESI-TOF) m/z: for ($C_{13}H_{11}Br_2N_2O_3S$ [M + H]$^+$) calcd, 432.8857; found, 432.8862. HPLC t_R = 7.53 min.

2,4-Dibromo-N-(4-(N-methylsulfamoyl)phenyl)benzamide (4d).

This product was synthesized using 2,4-dibromo benzoic acid (1b, 140 mg, 5 mmol) via its carboxylic acid chloride (2b) and 4-amino-*N*methylbenzenesulfonamide (3d, 102 mg, 5.5 mmol) in the presence of $NaHCO_3$ (172 mg, 20 mmol). Colorless solid. Yield: 53% (118 mg). mp: 221−223 °C. ^{1}H NMR (500 MHz, DMSO-d_6): δ 10.93 (s, 1H), 8.02 (t, J = 5.6 Hz, 1H), 7.92 (t, J = 8.0 Hz, 2H), 7.79−7.64 (m, 3H), 7.55 (d, J = 8.2 Hz, 1H), 2.59 (s, 3H). ^{13}C NMR (126 MHz, DMSO-d_6): δ 165.74, 137.88, 134.92, 131.70, 131.02, 130.74, 130.63, 130.47, 130.13, 129.54, 129.01, 128.79, 123.72, 120.26, 119.67, 37.78. HRMS (ESI-TOF) m/z: for ($C_{14}H_{13}Br_2N_2O_3S$ [M + H]$^+$) calcd, 446.9014; found, 446.9011. HPLC t_R = 7.84 min.

2,4-Dichloro-N-(4-(N,N-dimethylsulfamoyl)phenyl)benzamide (4e).

This product was synthesized using 2,4-dichlorobenzoic acid (1a, 95 mg, 5 mmol) via its carboxylic acid chloride (2a) and 4amino-*N*,*N*-dimethylbenzenesulfonamide (3e, 110 mg, 5.5 mmol) in the presence of $NaHCO_3$ (172 mg, 20 mmol). Yield: 25%. mp: 186− 188 °C. ^{1}H NMR (500 MHz, DMSO-d_6): δ (ppm) 10.95 (s, 1H), 8.00−7.87 (m, 2H), 7.84−7.71 (m, 3H), 7.66 (d, J = 8.3 Hz, 1H),

7.57 (dd, J = 8.1, 1.9 Hz, 1H), 2.59 (s, 6H). ^{13}C NMR (126 MHz, DMSO-d_6): δ (ppm) 164.76, 142.84, 135.42, 135.37, 131.40, 130.58, 129.54, 129.46, 129.00, 127.74, 119.68, 37.77. HRMS (ESI-TOF) m/z: for ($C_{15}H_{15}Cl_2N_2O_3S$ [M + H]$^+$) calcd, 373.0180; found, 373.0176. HPLC t_R = 7.92 min.

Synthesis of Sulfonamides (3f-i, 3k).[19]

At 0 °C, 4-acetamidobenzenesulfonyl chloride (5, 4.3 mmol) was dissolved in dichloromethane (80 mL). The solution received dropwise additions of trimethylamine (4.5 mmol, 1.05 equiv) and appropriate amine (8.6 mmol, 2 equiv). A further 2 h at room temperature were spent stirring the mixture. TLC monitored how the response changed. The mixture was then supplemented with brine solution and 2 N HCl following the process. After filtering the mixture to remove the residue, the solid was recovered. The

Published in : Journal of Agricultural and Food Chemistryl (2024), vol. 72, n°37, pp. 20670-20678
DOI: 10.1021/acs.jafc.4c05094
Status : Postprint (Author's version)

mixture was washed with water and dichloromethane to remove the residue. After being treated with concentrated HCl, the corresponding intermediate (6a-e) was refluxed and stirred for 2 h. The mixture was cleansed with NaOH after cooling to room temperature, and then methanol and dichloromethane (1:10) were used to extract the material. The combined organic layers were dried over magnesium sulfate and concentrated under vacuum. The crude products were purified by silica-gel column chromatography.

The data for 4-amino-*N*-(5-methylisoxazol-3-yl)benzenesulfonamide (3f),[30] 4-amino-*N*-(4,5-dimethylisoxazol-3-yl)benzenesulfonamide (3g),[30] 4-amino-*N*-(5-methyl-1,3,4-thiadiazol-2yl)benzenesulfonamide (3h),[31] 4-amino-*N*-(quinoxalin-2-yl)benzenesulfonamide (3i),[32] and 4-amino-*N*-phenylbenzenesulfonamide (3k)[19] are reported in the appropriate references.

Procedure A for the Synthesis of 7a-s.

The corresponding carboxylic acid chloride (2a, c-n) was synthesized according to the procedure for the synthesis of 2a,b. The resultant carboxylic acid chloride was then subjected to a treatment with 4-amino-*N*phenylsulfonamide derivatives (3f-i, 3k, 2 mmol), while $NaHCO_3$ (40 mmol) in acetone was present during an overnight period at room temperature. Acetone was evaporated when the reaction was finished, and the remaining substance was then added to freezing water. Ethyl acetate was then used to extract the mixture (3× 30 mL). The organic layer was recovered and then dried over magnesium sulfate before being concentrated under vacuum. By utilizing 40−50% ethyl acetate in petroleum ether, column chromatography was used to purify the product.

Procedure B for the Synthesis of 7t-z, 7aa-ai.

To the solution of the appropriate carboxylic acid (1p-z, 1aa-ad, 10 mmol) and the sulfonamide 3k (10 mmol) in THF (10 mL), 50% T3P in solution EA (30 mmol) was added, followed by pyridine (30 mmol). For 12 h, the mixture was heated to 50 °C. After the completion of the reaction, the mixture was poured into ice-cold water and extracted with EA (3× 30 mL). The combined organic layers were washed with 10% $NaHCO_3$ (2× 20 mL) and 2 N HCl (2× 20 mL), dried over magnesium sulfate, and concentrated under vacuum. The crude products were purified by silica-gel column chromatography.

2,4-Dichloro-N-(4-(N-(5-methylisoxazol-3-yl)sulfamoyl)phenyl)benzamide (7a).

This product was synthesized according to procedure A using 2,4-dichloro benzoic acid (1a, 189 mg, 10 mmol) and 4-amino-*N*-(5-methylisoxazol-3-yl)benzenesulfonamide (3f, 304 mg, 12 mmol) in the presence of $NaHCO_3$ (336 mg, 40 mmol). Colorless solid; yield 49% (208 mg); mp: 193−195 °C. ^{1}H NMR (400 MHz, DMSO-d_6): δ 10.83 (s, 1H), 7.84−7.71 (m, 5H), 7.64 (t, J = 9.3 Hz, 1H), 7.63−7.46 (m, 1H), 5.95 (s, 1H), 2.21 (s, 3H). ^{13}C NMR (101 MHz, DMSO): δ 168.16, 164.78, 141.45, 135.87, 135.52, 131.71, 130.85, 129.69, 127.97, 127.91, 119.53, 96.73, 12.60. HRMS (ESI-TOF) m/z: for ($C_{17}H_{14}Cl_2N_3O_4S$ [M + H]$^+$) calcd, 426.0082; found, 426.0086. HPLC t_R = 7.96 min.

Published in : Journal of Agricultural and Food Chemistryl (2024), vol. 72, n°37, pp. 20670-20678
DOI: 10.1021/acs.jafc.4c05094
Status : Postprint (Author's version)

2,4-Dichloro-N-(4-(N-(4,5-dimethylisoxazol-3-yl)sulfamoyl)phenyl)benzamide (7b).

This product was synthesized according to procedure A using 2,4-dichloro benzoic acid (1a, 189 mg, 10 mmol) and 4-amino-*N*-(4,5-dimethylisoxazol-3-yl)benzenesulfonamide (3g, 320 mg, 12 mmol) in the presence of $NaHCO_3$ (336 mg, 40 mmol). Colorless solid; yield 58% (255 mg); mp: 178−180 °C. ^{1}H NMR (400 MHz, DMSO-d_6): δ 10.67 (s, 1H), 7.72−7.70 (m, 5H), 7.64− 7.29 (m, 2H), 1.89 (s, 3H), 1.58 (s, 3H). ^{13}C NMR (101 MHz, DMSO): δ 173.29, 164.69, 130.83, 129.64, 127.92, 127.26, 119.07, 102.67, 10.99, 7.19. HRMS (ESI-TOF) *m*/*z*: for ($C_{18}H_{16}Cl_2N_3O_4S$ $[M + H]^+$) calcd, 440.0239; found, 440.0235. HPLC t_R = 8.10 min.

2,4-Dichloro-N-(4-(N-(5-methyl-1,3,4-thiadiazol-2-yl)sulfamoyl)phenyl)benzamide (7c).

This product was synthesized according to procedure A using 2,4-dichloro benzoic acid (1a, 189 mg, 10 mmol) and 4-amino-*N*-(5-methyl-1,3,4-thiadiazol-2-yl)benzenesulfonamide (3h, 270 mg, 12 mmol) in the presence of $NaHCO_3$ (336 mg, 40 mmol). Colorless solid; yield 79% (350 mg); mp: >250 °C. ^{1}H NMR (400 MHz, DMSO-d_6): δ 10.71 (s, 1H), 7.76 (d, *J* = 1.9 Hz, 1H), 7.67 (dt, *J* = 13.9, 8.7 Hz, 5H), 7.55 (dd, *J* = 8.2, 2.0 Hz, 1H), 2.35 (s, 3H). ^{13}C NMR (101 MHz, DMSO): δ 169.27, 164.62, 153.66, 141.31, 140.55, 136.01, 135.41, 131.71, 130.83, 129.66, 127.93, 127.31, 119.21, 16.09. HRMS (ESI-TOF) *m*/*z*: for ($C_{16}H_{13}Cl_2N_4O_3S_2$ $[M + H]^+$) calcd, 442.9806; found, 442.9802. HPLC t_R = 7.65 min.

2,4-Dichloro-N-(4-(N-(quinoxalin-2-yl)sulfamoyl)phenyl)benzamide (7d).

This product was synthesized according to procedure A using 2,4-dichloro benzoic acid (1a, 189 mg, 10 mmol) and 4-amino-*N*-(quinoxalin-2-yl)benzenesulfonamide (3i, 360 mg, 12 mmol) in the presence of $NaHCO_3$ (336 mg, 40 mmol). Colorless powder; yield 63% (298 mg); mp: 208−210 °C. ^{1}H NMR (400 MHz, DMSO-d_6): δ 12.04 (s, 1H), 10.92 (s, 1H), 8.63 (s, 1H), 8.12−8.09 (m, 3H), 7.92−7.90 (m, 5H), 7.59−7.56 (m, 3H). ^{13}C NMR (101 MHz, DMSO): δ 166.68, 164.87, 146.65, 143.20, 135.65, 131.68, 131.40, 130.85, 129.72, 129.22, 127.97, 127.70, 127.62, 119.54. HRMS (ESI-TOF) *m*/*z*: for ($C_{21}H_{15}Cl_2N_4O_3S$ $[M + H]^+$) calcd, 473.0242; found, 473.0237. HPLC t_R = 8.76 min.

N-(4-(N-Acetylsulfamoyl)phenyl)-2,4-dichlorobenzamide (7e).

This product was synthesized according to procedure A using 2,4dichloro benzoic acid (1a, 189 mg, 10 mmol) and *N*-((4aminophenyl)sulfonyl)acetamide (3j, 250 mg, 12 mmol) in the presence of $NaHCO_3$ (336 mg, 40 mmol). Colorless powder; yield 71% (275 mg); mp: 227−229 °C. ^{1}H NMR (400 MHz, DMSO-d_6): δ 10.97 (s, 1H), 7.90 (s, 4H), 7.80 (d, *J* = 1.8 Hz, 1H), 7.68 (d, *J* = 8.2 Hz, 1H), 7.59 (dd, *J* = 8.2, 1.9 Hz, 1H), 1.89 (d, *J* = 12.6 Hz, 3H). ^{13}C NMR (101 MHz, DMSO): δ 169.61, 165.02, 143.34, 135.68, 134.89, 131.71, 130.87, 129.75, 129.33, 128.02, 119.60, 23.92. HRMS (ESITOF) *m*/*z*: for ($C_{15}H_{13}Cl_2N_4O_4S$ $[M + H]^+$) calcd, 386.9973; found, 386.9965. HPLC t_R = 8.10 min.

2,4-Dibromo-N-(4-(N-phenylsulfamoyl)phenyl)benzamide (7f).

This product was synthesized according to procedure A using 2,4dibromo benzoic acid (5a, 297 mg, 10 mmol) and the amine 3k (297 mg, 12 mmol) in the presence of $NaHCO_3$ (336 mg, 40 mmol). Colorless solid; yield 87% (443 mg); mp: 233−235 °C. ^{1}H NMR (400 MHz, DMSO-d_6): δ 10.89 (s, 1H, NH), 10.24 (s,

Published in : Journal of Agricultural and Food Chemistryl (2024), vol. 72, n°37, pp. 20670-20678
DOI: 10.1021/acs.jafc.4c05094
Status : Postprint (Author's version)

1H, NH), 7.90 (d, *J* = 0.7 Hz, 1H), 7.82 (d, *J* = 8.8 Hz, 2H), 7.75 (d, *J* = 8.8 Hz, 2H), 7.61 (d, *J* = 1.5 Hz, 2H), 7.23 (t, *J* = 7.9 Hz, 2H), 7.10 (d, *J* = 7.6 Hz, 2H), 7.02 (t, *J* = 7.3 Hz, 1H). ^{13}C NMR (101 MHz, DMSO-d_6): δ 165.89, 142.91, 138.38, 137.85, 135.57, 134.65, 132.54, 130.69, 129.61, 128.47, 128.38, 124.35, 120.38, 119.80. HRMS (ESI-TOF) *m/z*: for ($C_{19}H_{15}Br_2N_2O_3S$ [M + H]$^+$) calcd, 508.9170; found, 508.9174. HPLC t_R = 7.96 min.

2,4-Difluoro-N-(4-(N-phenylsulfamoyl)phenyl)benzamide (7g).

This product was synthesized according to procedure A using 2,4difluorobenzoic acid (5b, 158 mg, 10 mmol) and 3k (297 mg, 12 mmol) in the presence of $NaHCO_3$ (336 mg, 40 mmol).

Colorless solid; yield 84% (326 mg); mp: 184−186 °C. ^{1}H NMR (400 MHz, DMSO-d_6): δ 10.77 (s, 1H, NH), 7.81 (t, *J* = 10.0 Hz, 2H), 7.75−7.72 (m, 3H), 7.43−7.41 (m, 1H), 7.30−7.15 (m, 3H), 7.07 (t, *J* = 7.9 Hz, 2H), 7.00 (d, *J* = 7.4 Hz, 1H). ^{13}C NMR (101 MHz, DMSO-d_6): δ 162.05 (d, *J* = 158.5 Hz), 162.84, 160.07 (d, *J* = 239.2 Hz), 142.77, 139.02, 135.13, 132.20 (dd, *J* = 10.4, 4.2 Hz), 129.42 (d, *J* = 13.1 Hz), 129.12, 128.33, 123.97, 120.58, 119.93, 112.37 (d, *J* = 18.2 Hz), 105.43, 105.04 (d, *J* = 26.3 Hz). HRMS (ESITOF) *m/z*: for ($C_{19}H_{14}F_2N_2NaO_3S$ [M + Na]$^+$) calcd, 411.0591; found, 411.0595. HPLC t_R = 6.46 min.

2,4-Dimethyl-N-(4-(N-phenylsulfamoyl)phenyl)benzamide (7h).

This product was synthesized according to procedure A using 2,4dimethylbenzoic acid (5c, 198 mg, 10 mmol) and 3k (297 mg, 12 mmol) in the presence of $NaHCO_3$ (336 mg, 40 mmol). Colorless solid; yield 81% (307 mg); mp: 191−193 °C. ^{1}H NMR (400 MHz, DMSO-d_6): δ 10.53 (s, 1H), 7.82 (d, *J* = 8.6 Hz, 2H), 7.78−7.63 (m, 2H), 7.37 (t, *J* = 6.9 Hz, 1H), 7.13 (dd, *J* = 8.6, 8.9 Hz, 4H), 7.04 (d, *J* = 7.0 Hz, 2H), 6.91 (s, 1H), 2.33 (s, 3H), 2.31 (s, 3H). ^{13}C NMR (101 MHz, DMSO-d_6): δ 168.66, 142.76, 140.07, 136.03, 134.20, 131.70, 129.25, 128.04, 127.93, 126.54, 120.54, 119.60, 21.25, 19.77. HRMS (ESI-TOF) *m/z*: for ($C_{21}H_{20}F_2N_2NaO_3S$ [M + Na]$^+$) calcd, 403.1092; found, 403.1090. HPLC t_R = 8.12 min.

N-(4-(N-Phenylsulfamoyl)phenyl)-2,4-bis(trifluoromethyl)benzamide (7i).

This product was synthesized according to procedure A using 2,4-di(trifluoromethyl)benzoic acid (5d, 258 mg, 10 mmol) and 3k (297 mg, 12 mmol) in the presence of $NaHCO_3$ (336 mg, 40 mmol). Brown solid; yield 76% (370 mg); mp: 216−218 °C. ^{1}H NMR (400 MHz, DMSO-d_6): δ 11.06 (s, 1H, NH), 10.28 (s, 1H, NH), 8.24 (d, *J* = 11.4 Hz, 2H), 8.02 (d, *J* = 7.9 Hz, 1H), 7.89− 7.59 (m, 4H), 7.22 (t, *J* = 7.9 Hz, 2H), 7.09 (d, *J* = 7.7 Hz, 2H), 6.99 (t, *J* = 7.4 Hz, 1H). ^{13}C NMR (101 MHz, DMSO-d_6): δ 165.12, 142.47, 139.66, 138.99, 135.48, 131.28, 130.20 (q, *J* = 188.3 Hz), 129.54, 128.47, 126.11 (q, *J* = 264.3 Hz), 124.90, 124.69, 123.93, 120.43, 119.90. HRMS (ESI-TOF) *m/z*: for ($C_{21}H_{15}F_6N_2O_3S$ [M + H]$^+$) calcd, 489.0708; found, 489.0703. HPLC t_R = 8.77 min.

2-Chloro-N-(4-(N-phenylsulfamoyl)phenyl)-4-(trifluoromethyl)benzamide (7j).

This product was synthesized according to procedure A using 2-chloro-4-(trifluoromethyl)benzoic acid (5e, 224 mg, 10 mmol) and 3k (297 mg, 12 mmol) in the presence of $NaHCO_3$ (336 mg, 40 mmol). Brown solid; yield 77% (349 mg); mp: 210−212 °C. ^{1}H NMR (400 MHz, DMSO-d_6): δ 10.93 (s, 1H, NH), 8.11−7.93

Published in : Journal of Agricultural and Food Chemistryl (2024), vol. 72, n°37, pp. 20670-20678
DOI: 10.1021/acs.jafc.4c05094
Status : Postprint (Author's version)

(m, 1H), 7.84 (d, *J* = 8.6 Hz, 2H), 7.75 (q, *J* = 8.8 Hz, 4H), 7.11 (t, *J* = 7.7 Hz, 2H), 6.98 (d, *J* = 7.9 Hz, 2H), 6.81 (t, *J* = 6.7 Hz, 1H). ^{13}C NMR (101 MHz, DMSO-d_6): δ 164.53, 141.42, 140.73, 131.44, 130.42, 129.11, 128.15, 127.06 (d, *J* = 3.8 Hz), 124.88 (q, *J* = 3.8 Hz), 121.04 (d, *J* = 229.7 Hz), 119.60. HRMS (ESI-TOF) *m*/*z*: for ($C_{20}H_{15}ClF_3N_2O_3S$ [M + H]$^+$) calcd, 455.0444; found, 455.0437. HPLC t_R = 8.12 min.

2-Chloro-4-methoxy-N-(4-(N-phenylsulfamoyl)phenyl)benzamide (7k).

This product was synthesized according to procedure A using 2-chloro-4-methoxybenzoic acid (5f, 186 mg, 10 mmol) and 3k (297 mg, 12 mmol) in the presence of $NaHCO_3$ (336 mg, 40 mmol). Brown solid; yield 80% (332 mg); mp: 164−166 °C. ^{1}H NMR (400 MHz, DMSO-d_6): δ 10.75 (s, 1H, NH), 10.22 (s, 1H, NH), 7.83 (d, *J* = 8.9 Hz, 2H), 7.78−7.67 (m, 2H), 7.56 (s, 1H), 7.23−7.21 (m, 2H), 7.15 (d, *J* = 2.5 Hz, 1H), 7.13−7.06 (m, 2H), 7.06−6.95 (m, 2H), 3.83 (s, 3H). ^{13}C NMR (101 MHz, DMSO-d_6): δ 165.71, 161.42, 143.29, 138.27, 134.19, 131.82, 130.85, 129.61, 129.00, 128.41, 124.43, 120.41, 119.68, 115.46, 113.56, 56.37. HRMS (ESI-TOF) *m*/*z*: for ($C_{20}H_{18}ClN_2O_4S$ [M + H]$^+$) calcd, 417.0607; found, 417.0611. HPLC t_R = 7.46 min.

2-Chloro-4-cyano-N-(4-(N-phenylsulfamoyl)phenyl)benzamide (7l).

This product was synthesized according to procedure A using 2chloro-4-cyanobenzoic acid (5g, 181 mg, 10 mmol) and 3k (297 mg, 12 mmol) in the presence of $NaHCO_3$ (336 mg, 40 mmol). Brown solid; yield 78% (320 mg); mp: 202−204 °C. ^{1}H NMR (400 MHz, DMSO-d_6): δ 11.02 (s, 1H, NH), 8.22 (d, *J* = 8.0 Hz, 1H), 7.97 (dd, *J* = 7.9, 1.3 Hz, 1H), 7.88−7.82 (m, 2H), 7.81−7.62 (m, 3H), 7.18 (t, *J* = 7.8 Hz, 2H), 7.05 (d, *J* = 7.8 Hz, 2H), 6.94 (t, *J* = 7.2 Hz, 1H). ^{13}C NMR (101 MHz, DMSO-d_6): δ 164.43, 140.98, 133.69, 131.92, 131.30, 130.25, 129.43, 128.39, 120.50, 119.80, 117.58, 114.33. HRMS (ESI-TOF) *m*/*z*: for ($C_{20}H_{14}ClN_3NaO_3S$ [M + Na]$^+$) calcd, 434.0342; found, 434.0336. HPLC t_R = 6.62 min.

2-Bromo-4-methoxy-N-(4-(N-phenylsulfamoyl)phenyl)benzamide (7m).

This product was synthesized according to procedure A using 2-bromo-4-methoxybenzoic acid (5h, 231 mg, 10 mmol) and 3k (297 mg, 12 mmol) in the presence of $NaHCO_3$ (336 mg, 40 mmol). Brown solid; yield 82% (372 mg); mp: 203−205 °C. ^{1}H NMR (400 MHz, DMSO-d_6): δ 10.73 (s, 1H, NH), 10.20 (s, 1H, NH), 7.83 (d, *J* = 8.8 Hz, 2H), 7.74 (d, *J* = 8.9 Hz, 2H), 7.51 (d, *J* = 8.5 Hz, 1H), 7.28 (d, *J* = 2.4 Hz, 1H), 7.27−7.16 (m, 2H), 7.16− 7.08 (m, 2H), 7.08−6.95 (m, 2H), 3.83 (s, 3H). ^{13}C NMR (101 MHz, DMSO-d_6): δ 166.55, 161.27, 143.31, 138.31, 131.25, 130.66, 129.58, 128.36, 124.41, 120.47, 119.71, 118.51, 113.96, 56.36. HRMS (ESI-TOF) *m*/*z*: for ($C_{20}H_{17}BrN_2NaO_4S$ [M + Na]$^+$) calcd, 482.9990; found, 482.9982. HPLC t_R = 7.04 min.

2-Bromo-N-(4-(N-phenylsulfamoyl)phenyl)-4-(trifluoromethyl)benzamide (7n).

This product was synthesized according to procedure A using 2-bromo-4-(trifluoromethyl)benzoic acid (5i, 0.269 mg, 10 mmol) and 3k (297 mg, 12 mmol) in the presence of $NaHCO_3$ (336 mg, 40 mmol). Brown solid; yield 77% (384 mg); mp: 218−220 °C. ^{1}H NMR (400 MHz, DMSO-d_6): δ 10.98 (s, 1H, NH), 10.30 (s, 1H, NH), 8.16 (s, 1H), 7.90 (d, *J* = 7.9 Hz, 1H), 7.86−7.79 (m, 3H), 7.76 (d, *J* = 8.8 Hz, 2H), 7.21 (t, *J* = 7.5 Hz, 2H), 7.08 (d, *J* = 8.1 Hz, 2H), 6.98 (t, *J* = 6.8 Hz, 1H). ^{13}C NMR (101 MHz, DMSO-d_6): δ 165.12, 142.65 (d, *J*

Published in : Journal of Agricultural and Food Chemistryl (2024), vol. 72, n°37, pp. 20670-20678
DOI: 10.1021/acs.jafc.4c05094
Status : Postprint (Author's version)

= 38.4 Hz), 130.20, 129.91 (d, *J* = 8.1 Hz), 128.40, 125.33 (d, *J* = 5.4 Hz), 120.51, 120.17, 119.84. HRMS (ESI-TOF) *m*/*z*: for ($C_{20}H_{14}BrF_3N_2NaO_3S$ [M + Na]$^+$) calcd, 520.9758; found, 520.9749. HPLC t_R = 8.63 min.

4-Methoxy-2-methyl-N-(4-(N-phenylsulfamoyl)phenyl)benzamide (7o).

This product was synthesized according to procedure A using 4-methoxy-2-methylbenzoic acid (5j, 0.166 mg, 10 mmol) and 3k (297 mg, 12 mmol) in the presence of $NaHCO_3$ (336 mg, 40 mmol). Brown solid; yield 74% (294 mg); mp: 190−192 °C. ^{1}H NMR (400 MHz, DMSO-d_6): δ 10.63 (s, 1H, NH), 10.19 (s, 1H, NH), 7.81 (d, *J* = 8.6 Hz, 2H), 7.70 (d, *J* = 8.8 Hz, 2H), 7.49 (d, *J* = 8.0 Hz, 1H), 7.40 (s, 1H), 7.36 (dd, *J* = 8.0, 2.0 Hz, 1H), 7.21 (t, *J* = 8.0 Hz, 2H), 7.13−7.03 (m, 2H), 7.02 (t, *J* = 7.6 Hz, 1H), 3.85 (s, OCH_3), 2.35 (s, 3H). ^{13}C NMR (101 MHz, DMSO-d_6): δ 167.44, 143.02, 138.39, 138.21, 138.02, 135.41, 134.61, 134.04, 130.42, 129.40, 129.30, 128.05, 125.79, 124.10, 120.10, 119.58, 56.84, 18.30. HRMS (ESI-TOF) *m*/*z*: for ($C_{21}H_{21}N_2O_4S$ [M + H]$^+$) calcd, 397.1222; found, 397.1225. HPLC t_R = 8.60 min.

2 - Methoxy-N-(4-(N-phenylsulfamoyl)phenyl) - 4 (trifluoromethyl)benzamide (7p).

This product was synthesized according to procedure A using 2-methoxy-4-(trifluoromethyl)benzoic acid (5k, 0.220 mg, 10 mmol) and 3k (297 mg, 12 mmol) in the presence of $NaHCO_3$ (336 mg, 40 mmol). Brown solid; yield 83% (373 mg); mp: 223−225 °C. ^{1}H NMR (400 MHz, DMSO-d_6): δ 10.63 (s, 1H, NH), 10.20 (s, 1H, NH), 7.83 (d, *J* = 8.2 Hz, 2H), 7.79−7.58 (m, 3H), 7.53−7.30 (m, 2H), 7.23 (t, *J* = 7.5 Hz, 2H), 7.10 (d, *J* = 8.2 Hz, 2H), 7.02 (t, *J* = 6.9 Hz, 1H), 3.93 (s, 3H). ^{13}C NMR (101 MHz, DMSO-d_6): δ 164.85, 157.39, 143.03, 138.28, 134.37, 130.48, 129.60, 128.42, 124.41, 120.46, 119.76, 117.59 (t, *J* = 3.9 Hz), 109.24 (t, *J* = 4.9 Hz), 56.86. HRMS (ESI-TOF) *m*/*z*: for ($C_{21}H_{17}F_3N_2NaO_4S$ [M + Na]$^+$) calcd, 473.0759; found, 473.0750. HPLC t_R = 8.09 min.

4-Chloro-N-(4-(N-phenylsulfamoyl)phenyl)-2-(trifluoromethoxy)benzamide (7q).

This product was synthesized according to procedure A using 4-chloro-2-(trifluoromethoxy)benzoic acid (5l, 0.240 mg, 10 mmol) and 3k (297 mg, 12 mmol) in the presence of $NaHCO_3$ (336 mg, 40 mmol). Brown solid; yield 76% (357 mg); mp: 195−197 °C. ^{1}H NMR (400 MHz, DMSO-d_6): δ 10.93 (s, 1H, NH), 7.97 (s, 1H), 7.91 (d, *J* = 8.2 Hz, 1H), 7.88−7.62 (m, 5H), 7.15 (t, *J* = 7.6 Hz, 2H), 7.02 (d, *J* = 7.8 Hz, 2H), 6.89 (t, *J* = 6.9 Hz, 1H). ^{13}C NMR (101 MHz, DMSO-d_6): δ 165.36, 141.89, 135.38, 133.12, 131.16, 129.32, 128.25, 126.92, 123.27 (d, *J* = 274.0 Hz), 122.60 (q, *J* = 17.0 Hz), 120.51, 119.72. HRMS (ESI-TOF) *m*/*z*: for ($C_{20}H_{14}ClF_3N_2NaO_4S$ [M + Na]$^+$) calcd, 493.0213; found, 493.0215. HPLC t_R = 7.98 min.

4-Chloro-2-methoxy-N-(4-(N-phenylsulfamoyl)phenyl)benzamide (7r).

This product was synthesized according to procedure A using 4-chloro-2-methoxybenzoic acid (5m, 186 mg, 10 mmol) and 3k (297 mg, 12 mmol) in the presence of $NaHCO_3$ (336 mg, 40 mmol). Brown solid; yield 80% (332 mg); mp: 207−209 °C. ^{1}H NMR (400 MHz, DMSO-d_6): δ 10.40 (s, 1H), 10.14 (s, 1H), 7.80 (d, *J* = 8.8 Hz, 2H), 7.75−7.62 (m, 2H), 7.51 (d, *J* = 8.0 Hz, 1H), 7.36 (t, *J* = 8.2 Hz, 1H), 7.29−7.15 (m, 3H), 7.15−7.06 (m, 2H), 7.04−6.87 (m, 1H), 3.87 (s, 3H). ^{13}C NMR (101 MHz, DMSOd_6): δ 164.54, 157.30, 142.79, 137.98, 133.96, 131.23, 129.21, 125.25, 124.21, 124.19, 123.53, 120.27, 119.68, 115.57, 56.24. HRMS (ESITOF) *m*/*z*: for ($C_{20}H_{17}ClN_2NaO_4S$ [M + Na]$^+$) calcd, 439.0495; found, 439.0485. HPLC t_R = 7.83 min. *(E)*-

Published in : Journal of Agricultural and Food Chemistryl (2024), vol. 72, n°37, pp. 20670-20678
DOI: 10.1021/acs.jafc.4c05094
Status : Postprint (Author's version)

*3-(2,4-Dichlorophenyl)-N-(4-(N-phenylsulfamoyl)phenyl)acrylamide (**7s**).* This product was synthesized according to procedure A using (*E*)-3-(2,4-dichlorophenyl)acrylic acid (1o, 217 mg, 10 mmol) and 3k (297 mg, 12 mmol) in the presence of $NaHCO_3$ (336 mg, 40 mmol). Brown solid; mp: >250 °C. Yield 65% (290 mg); ^{1}H NMR (400 MHz, DMSO-d_6): δ 10.68 (s, 1H), 10.19 (s, 1H), 7.86−7.78 (m, 4H), 7.78−7.69 (m, 3H), 7.55 (dd, *J* = 8.5, 2.0 Hz, 1H), 7.23 (t, *J* = 7.9 Hz, 2H), 7.13−7.06 (m, 2H), 7.02 (t, *J* = 7.4 Hz, 1H), 6.89 (d, *J* = 15.6 Hz, 1H). ^{13}C NMR (101 MHz, DMSO): δ 163.81, 143.25, 138.27, 135.54, 135.48, 134.81, 134.18, 131.87, 130.05, 129.59, 129.55, 128.66, 128.49, 125.92, 124.43, 120.47, 119.53. HRMS (ESI-TOF) *m*/*z*: for ($C_{21}H_{17}Cl_2N_2O_3S$ [M + H]$^+$) calcd, 447.0337; found, 447.0331. HPLC t_R = 8.16 min.

2,3,4-Trichloro-N-(4-(N-phenylsulfamoyl)phenyl)benzamide (7t).

This product was synthesized according to procedure B using 2,3,4trichlorobenzoic acid (5n, 225 mg, 10 mmol) and 3k (248 mg, 10 mmol) in the presence of T3P (1.9 mL, 30 mmol) and pyridine (0.242 mL, 30 mmol). Brown solid; yield 82% (373 mg); mp: 225− 227 °C. ^{1}H NMR (400 MHz, DMSO-d_6): δ 11.03 (s, 1H, NH), 10.31 (s, 1H, NH), 8.02 (s, 1H), 7.93−7.51 (m, 5H), 7.23 (t, *J* = 7.6 Hz, 2H), 7.10 (d, *J* = 7.7 Hz, 2H), 7.01 (t, *J* = 7.1 Hz, 1H). ^{13}C NMR (101 MHz, DMSO-d_6): δ 163.65, 142.60, 139.79, 138.50, 134.95, 133.73, 133.05, 131.47, 129.60, 128.52, 127.91, 127.76, 124.29, 120.41, 119.88. HRMS (ESI-TOF) *m*/*z* : for ($C_{19}H_{13}Cl_3N_2NaO_3S$ [M + Na]$^+$) calcd, 476.9610; found, 476.9614. HPLC t_R = 8.92 min.

2,4,5-Trichloro-N-(4-(N-phenylsulfamoyl)phenyl)benzamide (7u).

This product was synthesized according to procedure B using 2,4,5-trichlorobenzoic acid (5o, 225 mg, 10 mmol) and 3k (248 mg, 10 mmol) in the presence of T3P (1.9 mL, 30 mmol) and pyridine (0.242 mL, 30 mmol). Brown solid; yield 74% (336 mg); mp: 210− 212 °C. ^{1}H NMR (400 MHz, DMSO-d_6): δ 10.96 (s, 1H, NH), 10.24 (s, 1H, NH), 8.03 (s, 2H), 7.81 (d, *J* = 8.5 Hz, 2H), 7.76 (d, *J* = 8.5 Hz, 2H), 7.23 (t, *J* = 7.6 Hz, 2H), 7.10 (d, *J* = 7.7 Hz, 2H), 7.02 (t, *J* = 7.1 Hz, 1H). ^{13}C NMR (101 MHz, DMSO-d_6): δ 163.58, 142.73, 138.27, 136.76, 134.73, 133.85, 131.71, 130.23 (d, *J* = 8.3 Hz), 130.14, 129.61, 128.50, 124.44, 120.43, 119.89. HRMS (ESI-TOF) *m*/*z*: for ($C_{19}H_{13}Cl_3N_2NaO_3S$ [M + Na]$^+$) calcd, 476.9610; found, 476.9596. HPLC t_R = 8.48 min.

2,4,6-Trichloro-N-(4-(N-phenylsulfamoyl)phenyl)benzamide (7v).

This product was synthesized according to procedure B using 2,4,6-trichlorobenzoic acid (5p, 225 mg, 10 mmol) and 3k (248 mg, 10 mmol) in the presence of T3P (1.9 mL, 30 mmol) and pyridine (0.242 mL, 30 mmol). Brown solid; yield 73% (332 mg); mp: 188− 190 °C. ^{1}H NMR (400 MHz, DMSO-d_6): δ 10.88 (s, 1H), 10.22 (s, 1H), 7.94−7.92 (m, 1H), 7.88−7.80 (m, 2H), 7.81−7.69 (m, 3H), 7.23 (t, *J* = 7.9 Hz, 2H), 7.18−7.07 (m, 2H), 7.03 (d, *J* = 7.4 Hz, 1H). ^{13}C NMR (101 MHz, DMSO-d_6): δ 164.60, 142.54, 137.92, 135.31, 134.34, 131.34, 130.50, 129.37, 129.24, 128.10, 127.63, 124.10, 120.13, 119.50. HRMS (ESI-TOF) *m*/*z*: for ($C_{19}H_{13}Cl_3N_2NaO_3S$ [M + Na]$^+$) calcd, 476.9610; found, 476.9608. HPLC t_R = 8.50 min.

2,6-Dichloro-4-cyano-N-(4-(N-phenylsulfamoyl)phenyl)benzamide (7w).

This product was synthesized according to procedure B using 2,6-dichloro-4-cyanobenzoic acid (5q, 216 mg, 10 mmol) and 3k (248 mg, 10 mmol) in the presence of T3P (1.9 mL, 30 mmol) and pyridine (0.242

Published in : Journal of Agricultural and Food Chemistryl (2024), vol. 72, n°37, pp. 20670-20678
DOI: 10.1021/acs.jafc.4c05094
Status : Postprint (Author's version)

mL, 30 mmol). Brown solid; yield 71% (311 mg); mp: 183−185 °C. ^{1}H NMR (400 MHz, DMSO-d_6): δ ^{1}H NMR (400 MHz, DMSO-d_6): δ 11.07 (s, 2H), 8.75 (dd, J = 17.0, 2.0 Hz, 2H), 8.46 (dd, J = 15.7, 2.0 Hz, 2H), 7.88 (d, J = 8.8 Hz, 4H), 7.77 (d, J = 8.8 Hz, 4H), 7.38−7.16 (m, 4H), 7.10 (d, J = 7.6 Hz, 4H), 7.02 (t, J = 7.3 Hz, 3H). ^{13}C NMR (101 MHz, DMSO-d_6): δ 163.26, 149.28, 146.53, 142.53, 138.70, 138.37, 134.97, 133.30, 129.70, 129.60, 128.48, 124.41, 120.56, 120.05. HRMS (ESI-TOF) m/z: for ($C_{20}H_{14}Cl_2N_3O_3S$ [M + Na]$^+$) calcd, 446.0133; found, 446.0132. HPLC t_R = 7.80 min.

2,4-Dichloro-5-fluoro-N-(4-(N-phenylsulfamoyl)phenyl)benzamide (7x).

This product was synthesized according to procedure B using 2,4-dichloro-5-fluorobenzoic acid (5r, 209 mg, 10 mmol) and 3k (248 mg, 10 mmol) in the presence of T3P (1.9 mL, 30 mmol) and pyridine (0.242 mL, 30 mmol). Brown solid; yield 77% (350 mg); mp: 209−211 °C. ^{1}H NMR (400 MHz, DMSO-d_6): δ 10.92 (s, 1H), 10.27 (s, 1H), 7.99 (d, J = 6.5 Hz, 1H), 7.86 (d, J = 9.0 Hz, 1H), 7.77 (d, J = 8.8 Hz, 2H), 7.18−7.15 (m, 3H), 7.05 (d, J = 7.9 Hz, 2H), 6.94 (t, J = 7.2 Hz, 2H). ^{13}C NMR (101 MHz, DMSOd_6): δ 163.26, 156.38 (d, J = 248.4 Hz), 142.30, 137.13, 131.82, 129.41, 128.36, 126.64, 123.20, 122.51, 122.32, 120.52, 119.76, 117.97, 117.58. HRMS (ESI-TOF) m/z: for ($C_{19}H_{13}Cl_2FN_2NaO_3S$ [M + Na]$^+$) calcd, 460.9906; found, 460.9901. HPLC t_R = 8.44 min.

2,4-Difluoro-5-methyl-N-(4-(N-phenylsulfamoyl)phenyl)benzamide (7y).

This product was synthesized according to procedure B using 2,4-difluoro-5-methylbenzoic acid (5t, 172 mg, 10 mmol) and 3k (248 mg, 10 mmol) in the presence of T3P (1.9 mL, 30 mmol) and pyridine (0.242 mL, 30 mmol). Colorless solid; yield 79% (317 mg); mp: 199−201 °C. ^{1}H NMR (400 MHz, DMSOd_6): δ 10.74 (s, 1H, NH), 10.27 (s, 1H, NH), 7.87−7.78 (m, 2H), 7.78−7.70 (m, 2H), 7.64 (t, J = 8.3 Hz, 1H), 7.38 (t, J = 10.1 Hz, 1H), 7.27−7.17 (m, 2H), 7.14−7.07 (m, 2H), 7.06−6.97 (m, 1H), 2.28 (s, 3H). ^{13}C NMR (101 MHz, DMSO-d_6): δ 162.99, 160.16 (d, J = 246.7 Hz), 160.16 (d, J = 241.7 Hz), 143.02, 138.25, 134.40, 132.73, 129.61, 128.43, 124.46, 121.17 (dd, J = 41.0, 18.3 Hz), 120.49, 119.91, 105.78−102.77, 13.89. HRMS (ESI-TOF) m/z: for ($C_{20}H_{16}F_2N_2NaO_3S$ [M + Na]$^+$) calcd, 425.0747; found, 425.0741. HPLC t_R = 8.018 min.

2,5-Dichloro-4-methyl-N-(4-(N-phenylsulfamoyl)phenyl)benzamide (7z).

This product was synthesized according to procedure B using 2,5-dichloro-4-methylbenzoic acid (5t, 205 mg, 10 mmol) and 3k (248 mg, 10 mmol) in the presence of T3P (1.9 mL, 30 mmol) and pyridine (0.242 mL, 30 mmol). Brown solid; yield 71% (311 mg); mp: 199−201 °C. ^{1}H NMR (400 MHz, DMSO-d_6): δ 10.88 (s, 1H, NH), 10.26 (s, 1H, NH), 7.80 (s, 2H), 7.75−7.73 (m, 3H), 7.63 (s, 1H), 7.21 (t, J = 7.8 Hz, 2H), 7.08 (d, J = 7.7 Hz, 2H), 6.99 (t, J = 7.3 Hz, 1H), 2.37 (s, 3H). ^{13}C NMR (101 MHz, DMSOd_6): δ 164.33, 142.71, 139.75, 139.14, 135.62, 135.26, 132.43, 132.38, 129.48, 128.96, 128.33, 123.88, 120.54, 119.82, 19.69. HRMS (ESITOF) m/z: for ($C_{20}H_{16}Cl_2N_2NaO_3S$ [M + Na]$^+$) calcd, 457.0156; found, 457.0144. HPLC t_R = 8.62 min.

4,5-Dichloro-2-methyl-N-(4-(N-phenylsulfamoyl)phenyl)benzamide (7aa).

This product was synthesized according to procedure B using 4,5-dichloro-2-methylbenzoic acid (5u, 205 mg, 10 mmol) and 3k (248 mg, 10 mmol) in the presence of T3P (1.9 mL, 30 mmol) and pyridine (0.242 mL, 30 mmol). Brown solid; yield 75% (326 mg); mp 211−213 °C. ^{1}H NMR (400 MHz, DMSO-d_6): δ 10.77

Published in : Journal of Agricultural and Food Chemistryl (2024), vol. 72, n°37, pp. 20670-20678
DOI: 10.1021/acs.jafc.4c05094
Status : Postprint (Author's version)

(s, 1H, NH), 10.24 (s, 1H, NH), 7.84 (s, 2H), 7.80 (s, 1H), 7.75 (d, *J* = 8.8 Hz, 2H), 7.65 (s, 1H), 7.24 (t, *J* = 7.9 Hz, 2H), 7.11 (d, *J* = 7.7 Hz, 2H), 7.02 (t, *J* = 7.3 Hz, 1H), 2.35 (s, 3H). ^{13}C NMR (101 MHz, DMSO-d_6): δ 166.26, 143.14, 138.28, 137.40, 136.97, 134.38, 132.85, 132.80, 129.77, 129.62, 128.61, 128.37, 124.40, 120.33, 119.95, 18.95. HRMS (ESI-TOF) *m*/*z*: for ($C_{20}H_{16}Cl_2N_2NaO_3S$ [M + Na]$^+$) calcd, 457.0156; found, 457.0152. HPLC t_R = 8.04 min.

4-Chloro-2,5-dimethyl-N-(4-(N-phenylsulfamoyl)phenyl)benzamide (7ab).

This product was synthesized according to procedure B using 4-chloro-2,5-dimethylbenzoic acid (5v, 184 mg, 10 mmol) and 3k (248 mg, 10 mmol) in the presence of T3P (1.9 mL, 30 mmol) and pyridine (0.242 mL, 30 mmol). Brown solid; yield 81% (335 mg); mp 232−234 °C. ^{1}H NMR (400 MHz, DMSO-d_6): δ 10.68 (s, 1H, NH), 10.22 (s, 1H, NH), 7.85 (d, *J* = 8.8 Hz, 2H), 7.74 (d, *J* = 8.8 Hz, 2H), 7.49 (s, 1H), 7.40 (s, 1H), 7.24 (t, *J* = 7.9 Hz, 2H), 7.15−7.06 (m, 2H), 7.07−6.93 (m, 1H), 2.36 (s, 3H), 2.33 (s, 3H). ^{13}C NMR (101 MHz, DMSO-d_6): δ 167.77, 143.38, 138.30, 135.77, 135.61, 135.04, 134.14, 133.14, 131.11, 130.54, 129.62, 128.36, 124.40, 120.34, 119.79, 19.41, 18.98. HRMS (ESI-TOF) *m*/*z*: for ($C_{21}H_{20}ClN_2O_3S$ [M + H]$^+$) calcd, 415.0883; found, 415.0867. HPLC t_R = 8.48 min.

4-Bromo-2,5-dimethyl-N-(4-(N-phenylsulfamoyl)phenyl)benzamide (7ac).

This product was synthesized according to procedure B using 4-bromo-2,5-dimethylbenzoic acid (5w, 229 mg, 10 mmol) and 3k (248 mg, 10 mmol) in the presence of T3P (1.9 mL, 30 mmol) and pyridine (0.242 mL, 30 mmol). Brown solid; yield 70% (321 mg); mp 247−249 °C. ^{1}H NMR (400 MHz, DMSO-d_6): δ 10.68 (s, 1H, NH), 10.22 (s, 1H, NH), 7.79−7.77 (m, 4H), 7.48− 7.46 (m, 2H), 7.23 (d, *J* = 6.6 Hz, 2H), 7.07−7.05 (m, 3H), 2.36 (s, 3H), 2.33 (s, 3H). ^{13}C NMR (101 MHz, DMSO-d_6): δ 167.82, 143.36, 138.29, 136.19, 135.83, 135.04, 134.30, 134.15, 130.23, 129.62, 128.37, 126.07, 124.41, 120.35, 119.79, 22.22, 18.84. HRMS (ESI-TOF) *m*/*z*: for ($C_{21}H_{20}BrN_2O_3S$ [M + H]$^+$) calcd, 459.0378; found, 459.0383. HPLC t_R = 9.82 min.

4-Bromo-2-fluoro-5-methyl-N-(4-(N-phenylsulfamoyl)phenyl)benzamide (7ad).

This product was synthesized according to procedure B using 4-bromo-2-fluoro-5-methylbenzoic acid (5x, 233 mg, 10 mmol) and 3k (248 mg, 10 mmol) in the presence of T3P (1.9 mL, 30 mmol) and pyridine (0.242 mL, 30 mmol). Brown solid; yield 83% (384 mg); mp 225−227 °C. ^{1}H NMR (400 MHz, DMSOd_6): δ 11.00 (s, 1H, NH), 10.25 (s, 1H, NH), 7.82 (d, *J* = 8.9 Hz, 2H), 7.75 (d, *J* = 8.9 Hz, 2H), 7.56 (d, *J* = 8.8 Hz, 1H), 7.46 (s, 1H), 7.23 (t, *J* = 7.9 Hz, 2H), 7.10 (d, *J* = 7.6 Hz, 2H), 7.02 (t, *J* = 7.3 Hz, 1H), 2.30 (s, 3H). ^{13}C NMR (101 MHz, DMSO-d_6): δ 163.12, 158.81 (d, *J* = 249.3 Hz), 139.96 (d, *J* = 4.1 Hz), 138.25, 134.86, 129.53 (d, *J* = 13.1 Hz), 128.49, 125.26 (d, *J* = 18.4 Hz), 124.44, 122.91 (d, *J* = 11.0 Hz), 120.44, 119.78, 117.59−117.07, 116.92 (d, *J* = 25.2 Hz), 18.72. HRMS (ESI-TOF) *m*/*z*: for ($C_{20}H_{16}BrFN_2NaO_3S$ [M + Na]$^+$) calcd, 484.9947; found, 484.9941. HPLC t_R = 7.87 min.

2-Chloro-5-fluoro-4-methyl-N-(4-(N-phenylsulfamoyl)phenyl)benzamide (7ae).

This product was synthesized according to the procedure B using 2-chloro-5-fluoro-4-methylbenzoic acid (5y, 188 mg, 10 mmol) and 3k (248 mg, 10 mmol) in the presence of T3P (1.9 mL, 30 mmol) and pyridine (0.242 mL, 30 mmol). Brown solid; yield 72% (300 mg); mp 214−216 °C. ^{1}H NMR (400 MHz, DMSOd_6): δ

Published in : Journal of Agricultural and Food Chemistryl (2024), vol. 72, n°37, pp. 20670-20678
DOI: 10.1021/acs.jafc.4c05094
Status : Postprint (Author's version)

10.88 (s, 1H, NH), 10.24 (s, 1H, NH), 7.77−7.76 (m, 4H), 7.54 (dd, *J* = 7.1, 7.8 Hz, 2H), 7.24 (t, *J* = 7.7 Hz, 2H), 7.10 (d, *J* = 7.8 Hz, 2H), 7.03 (t, *J* = 7.2 Hz, 1H), 2.29 (s, 3H). ^{13}C NMR (101 MHz, DMSO-d_6): δ 164.54, 159.24 (d, *J* = 248.9 Hz), 142.97, 138.27, 135.55, 134.48, 132.89, 129.61, 128.83 (d, *J* = 19.0 Hz), 128.46, 125.64, 124.44, 120.43, 119.80, 116.21 (d, *J* = 25.7 Hz), 14.21. HRMS (ESI-TOF) *m*/*z*: for ($C_{20}H_{16}ClFN_2NaO_3S$ $[M + Na]^+$) calcd, 441.0452; found, 441.0446. HPLC t_R = 9.18 min.

4-Chloro-5-fluoro-2-methyl-N-(4-(N-phenylsulfamoyl)phenyl)benzamide (7af).

This product was synthesized according to procedure B using 4-chloro-5-fluoro-2-methylbenzoic acid (5z, 188 mg, 10 mmol) and 3k (248 mg, 10 mmol) in the presence of T3P (1.9 mL, 30 mmol) and pyridine (0.242 mL, 30 mmol). Brown solid; yield 78% (326 mg); mp 215−217 °C. ^{1}H NMR (400 MHz, DMSOd_6): δ 10.74 (s, 1H, NH), 10.23 (s, 1H, NH), 7.84 (d, *J* = 8.7 Hz, 2H), 7.75 (d, *J* = 8.7 Hz, 2H), 7.70−7.50 (m, 2H), 7.23 (t, *J* = 7.8 Hz, 2H), 7.10 (d, *J* = 7.7 Hz, 2H), 7.02 (t, *J* = 7.3 Hz, 1H), 2.33 (s, 3H). ^{13}C NMR (101 MHz, DMSO-d_6): δ 166.38, 155.44 (d, *J* = 240.4 Hz), 143.12, 138.32, 137.01, 134.01, 132.80, 129.61, 128.38, 124.37, 121.11 (d, *J* = 17.3 Hz), 120.34, 119.92, 116.47 (d, *J* = 22.4 Hz), 18.74. HRMS (ESI-TOF) *m*/*z*: for ($C_{20}H_{17}ClFN_2O_3S$ $[M + H]^+$) calcd, 419.0632; found, 419.0641. HPLC t_R = 8.11 min.

4-Bromo-5-fluoro-2-methyl-N-(4-(N-phenylsulfamoyl)phenyl)benzamide (7ag).

This product was synthesized according to procedure B using 4-bromo-5-fluoro-2-methylbenzoic acid (5aa, 233 mg, 10 mmol) and 3k (248 mg, 10 mmol) in the presence of T3P (1.9 mL, 30 mmol) and pyridine (0.242 mL, 30 mmol). Brown solid; yield 74% (342 mg); mp 229−231 °C. ^{1}H NMR (400 MHz, DMSOd_6): δ 10.73 (s, 1H, NH), 10.24 (s, 1H, NH), 7.83 (d, *J* = 8.8 Hz, 2H), 7.73 (d, *J* = 7.9 Hz, 3H), 7.57 (d, *J* = 9.0 Hz, 1H), 7.21 (t, *J* = 7.9 Hz, 2H), 7.08 (d, *J* = 7.6 Hz, 2H), 6.98 (t, *J* = 7.3 Hz, 1H), 2.34 (d, *J* = 8.7 Hz, 3H). ^{13}C NMR (101 MHz, DMSO-d_6): δ 166.43, 159.24 (d, *J* = 248.9 Hz), 157.85, 155.32, 142.89, 137.70, 135.61, 134.18, 129.52, 128.83 (d, *J* = 19.0 Hz), 123.84, 120.38, 119.87, 116.21 (d, *J* = 25.7 Hz), 109.65, 18.64. HRMS (ESI-TOF) *m*/*z*: for ($C_{20}H_{16}BrFN_2NaO_3S$ $[M + Na]^+$) calcd, 484.9947; found, 484.9940. HPLC t_R = 8.65 min.

4-Bromo-2,5-difluoro-N-(4-(N-phenylsulfamoyl)phenyl)benzamide (7ah).

This product was synthesized according to procedure B using 4-bromo-2,5-difluorobenzoic acid (5ab, 237 mg, 10 mmol) and 3k (248 mg, 10 mmol) in the presence of T3P (1.9 mL, 30 mmol) and pyridine (0.242 mL, 30 mmol). Brown solid; yield 79% (368 mg); mp 232−234 °C. ^{1}H NMR (400 MHz, DMSO-d_6): δ 10.88 (s, 1H, NH), 10.22 (s, 1H, NH), 7.95 (dd, *J* = 8.9, 5.5 Hz, 1H), 7.82 (d, *J* = 8.9 Hz, 2H), 7.80−7.67 (m, 3H), 7.23 (t, *J* = 7.9 Hz, 2H), 7.18−7.07 (m, 2H), 7.02 (t, *J* = 7.4 Hz, 1H). ^{13}C NMR (101 MHz, DMSO-d_6): δ 161.73, 155.14 (d, *J* = 252.67 Hz), 155.09 (d, *J* = 243.0 Hz), 142.69, 138.22, 134.73, 129.61, 128.47, 125.79−125.28, 124.49, 121.92 (d, *J* = 27.6 Hz), 120.53, 120.02, 117.66, 117.44, 111.75 (t, *J* = 12.4 Hz). HRMS (ESI-TOF) *m*/*z*: for ($C_{19}H_{13}BrF_2N_2NaO_3S$ $[M + Na]^+$) calcd, 488.9696; found, 488.9691. HPLC t_R = 8.00 min.

3-Chloro-N-(4-(N-phenylsulfamoyl)phenyl)-2-naphthamide (7ai).

This product was synthesized according to procedure B using 3chloro-2-naphthoic acid (5ac, 206 mg, 10 mmol) and 3k (248 mg, 10 mmol) in the presence of T3P (1.9 mL, 30 mmol) and pyridine (0.242 mL, 30 mmol). Brown solid; yield 74% (322 mg); mp 206− 208 °C. ^{1}H NMR (400 MHz, DMSO-d_6): δ 10.87 (s, 1H,

Published in : Journal of Agricultural and Food Chemistryl (2024), vol. 72, n°37, pp. 20670-20678
DOI: 10.1021/acs.jafc.4c05094
Status : Postprint (Author's version)

NH), 8.19 (s, 2H), 8.05 (d, *J* = 7.7 Hz, 1H), 7.98 (d, *J* = 7.8 Hz, 1H), 7.79 (d, *J* = 8.6 Hz, 2H), 7.75−7.68 (m, 2H), 7.64 (dd, *J* = 6.8, 5.7 Hz, 2H), 7.09 (d, *J* = 7.7 Hz, 2H), 6.95 (d, *J* = 7.8 Hz, 2H), 6.77 (d, *J* = 6.4 Hz, 1H). ^{13}C NMR (101 MHz, DMSO-d_6): δ 165.55, 134.61, 134.13, 131.26, 129.15, 128.83, 128.63, 128.36, 127.88, 127.69, 127.43, 120.78, 119.41. HRMS (ESI-TOF) *m*/*z*: for ($C_{23}H_{18}ClN_2O_3S$ [M + H]$^+$) calcd, 437.0727; found, 437.0732. HPLC t_R = 8.92 min.

Cell Culture, Plasmids, and Biological Evaluations.

All chemicals used were from Sigma-Aldrich (St. Louis, Missouri, USA) unless otherwise stated. Parental cell lines used for stable and transient transfection were HEK293-T (labeled as "HEK293" in the text, ATCC CRL-3216) and were obtained from the American Type Culture Collection (ATCC). Plasmids coding for GPR27V2-LFC, GPR27-LFC and βArr2-FLN are already described.[17] The pGloSensorTM-22F cAMP (cAMP GloSensor) plasmid was obtained from Promega Corporation (Madison, Wisconsin, USA). G_q-CASE (#168125), G_{i1}-CASE (#168120), G_{13}-CASE (#168127) plasmids were a gift from Gunnar Schulte obtained from Addgene (Watertown, Massachusetts, USA). Coding sequences for GPR27 and control receptors were obtained from plasmids from the cDNA Resource Center (Bloomsburg, Pennsylvania, USA). Cells were cultured at 37 °C in a humidified 5% CO2 incubator. HEK293 cells were grown in DMEM supplemented with 10% fetal bovine serum, 1% L-glutamine, 1% penicillin, and streptomycin. Stable cell lines (GPR27V2-LFC/ Arrb2-FLN, GPR27-LFC/Arrb2-FLN, and b2AR-LFC/Arrb2-FLN) culture medium was supplemented with puromycin (1 mg/mL) and hygromycin (200 mg/mL). A fresh culture medium supplemented with selection antibiotics was added to the cells the day before the experiment.

Measurement of β-Arrestin 2 Recruitment by Firefly Luciferase Complementation.

We used a previously described method[17,18] to measure the activity of compounds in HEK293 cells. Briefly, HEK293 cells stably expressing β-arrestin 2 fused with the N-terminal part of the firefly luciferase and $GPR27V_2$, GPR27, or β_2AR fused with the Cterminal part of the luciferase (HEK293.FnLArrb2.GPR27V2LFc and HEK293.FnLArrb2.GPR27LFc). To obtain concentration−response curves, 1 μL of a DMSO solution of the test compounds was added to white 96-well plates at appropriate concentrations. The cells were detached with trypsin, washed, and resuspended in HBSS (120 mM NaCl, 5.4 mM KCl, 0.8 mM $MgSO_4$, 10 mM HEPES; pH 7.4). Then, 100 μL of the cell suspension (at a final density of 35,000 cells/well) was added to each well (white LUMITRAC, Greiner Bio-One, Kremsmünster, Germany). The plates were incubated at room temperature for 10 min, and 100 μL of D-luciferin (at a concentration of 500 μM, Synchem, Felsberg, Germany) was added to each well. Luminescence was measured for 15 min immediately after the addition of D-luciferin (using a Centro XS3 LB960 plate reader (Berthold Technologies, Bad Wildbad, Germany).

Measurement of G Protein Dissociation by BRET.

The assay was adapted from Schihada et al. 2021.[29] Briefly, HEK293 cells were transfected with GPR27 or vector containing control receptors and the appropriate G-CASE plasmid with Mirus TransIT (Mirus bioLLC, Madison, Wisconsin) 48 h before the assay in 6 cm dishes. On the day of the experiment, cells were mixed with NLuc substrate, incubated for 5 min, and mixed with the compounds dissolved in DMSO

Published in : Journal of Agricultural and Food Chemistryl (2024), vol. 72, n°37, pp. 20670-20678
DOI: 10.1021/acs.jafc.4c05094
Status : Postprint (Author's version)

(final concentration: 1%). BRET was measured on a Flexstation 3 (Molecular Devices) with the monochromator set at 450 and 535 nm. The measurement length was 0.3 s per well. BRET ratios were determined by dividing the acceptor channel by the donor channel (Em_{535}/Em_{450}).

Determination of cAMP Levels. ALPHAScreen.

A detailed protocol for transient transfection with Lipofectamine 2000 (Thermo Fisher Scientific) and determination of cAMP content of cell extracts using a nonradioactive assay based on the ALPHAScreen technology (PerkinElmer LAS) has previously been published.[27]

GloSensor.

A detailed protocol has been published previously.[17,28] Briefly, HEK293 cells stably transfected with plasmid containing cAMP GloSensor and GPR27 were starved for 5 h with 1% FBS. Cells were detached and distributed into 96-well plates in HBSS (120 mM NaCl, 5.4 mM KCl, 0.8 mM $MgSO_4$, 10 mM HEPES; pH 7.4) containing IBMX (300 mM) (150,000 cells per well, white Lumitrac, Greiner Bio-One, Kremsmünster, Germany) containing the ligands at different concentrations in DMSO (max final concentration 1%). After 1 min agitation at 1200 rpm and 9 min incubation with compounds, luciferin was added, and the luminescence level was recorded for 15 min in a Centro XS3 LB960 plate reader (Berthold Technologies, Bad Wildbad, Germany).

Cell Viability Determination of Compounds 7p and 7af.

Confluent WT HEK293 in T75 flasks were detached with trypsin, washed, and resuspended in HBSS (120 mM NaCl, 5.4 mM KCl, 0.8 mM $MgSO_4$, 10 mM HEPES; pH 7.4). Then, 100 μL of the cell suspension (at a final density of ∼35,000 cells/well) was added to each well of a 96-well plate (white Lumitrac, Greiner Bio-One, Kremsmünster, Germany) containing the vehicle (DMSO) or compounds dissolved in DMSO (1 μL, final concentration <1%) at the indicated concentration. The plates were incubated at 37 °C for 60 min. Next, 100 μL of CellTiter-Glo one solution (Promega Corporation, Madison, Wisconsin, USA) was added and processed according to the manufacturer's instruction (10 min incubation at RT with shaking). The luminescence was read in a Berthold centro Xs luminometer plate reader (Berthold Technologies, Bad Wildbad, Germany) with a 0.5 s read per well.

Metabolic Stability in MLM/HLM.

Pooled liver microsomes from mice (male) and humans (male) were purchased from Sekisui XenoTech, LLC, Kansas City, KS, USA. Metabolic stability assays were performed in the presence of an NADPH-regenerating system consisting of 5 mM glucose-6-phosphate, 5 U/mL glucose-6phosphate dehydrogenase, and 1 mM $NADP^+$. Liver microsomes (20 mg/mL), NADPH-regenerating system, and 4 mM $MgCl_2 \cdot 6H_2O$ in 0.1 M Tris−HCl-buffer (pH 7.4) were preincubated for 5 min at 37 °C and 750 rpm on a shaker. The reaction was started by adding the preheated compound at 10 mM resulting in a final concentration of 0.1 mM. The reaction was quenched at selected time points (0, 10, 20, 30, 60, and 120 min) by pipetting 100 μL of internal standard (ketoprofen) at a concentration of 200 μM in acetonitrile.

Published in : Journal of Agricultural and Food Chemistryl (2024), vol. 72, n°37, pp. 20670-20678
DOI: 10.1021/acs.jafc.4c05094
Status : Postprint (Author's version)

The samples were vortexed for 30 s and centrifuged (21,910 relative centrifugal force, 4 °C, 20 min). The supernatant was used directly for LC−MS analysis.

All compound incubations were conducted at least in triplicate. Additionally, a negative control containing BSA (20 mg/mL) instead of liver microsomes and a positive control using Verapamil instead of compound were performed. A limit of 1% organic solvent during incubation was not exceeded.

Sample separation and detection were performed on an Alliance 2695 Separations Module HPLC system (Waters Corporation, Milford, MA, USA) equipped with a Phenomenex Kinetex 2.6 μm XB-C18 100 Å 50 × 3 mm column (Phenomenex Inc., Torrance, CA, USA) coupled to an Alliance 2996 Photodiode Array Detector and a MICROMASS QUATTRO micro API mass spectrometer (both Waters Corporation, Milford, MA, USA) using electrospray ionization in positive mode.

Mobile phase A: 90% water, 10% acetonitrile and additionally 0.1% formic acid (v/v), mobile phase B: 100% acetonitrile with additional 0.1% formic acid (v/v). The gradient was set to 0−2.5 min 10% B, 2.5−10 min from 10 to 80% B, 10−12 min 80% B, 12−12.01 min from 80 to 10% B, 12.01−17 min 10% B at a flow rate of 0.7 mL/min.

Samples were maintained at 10 °C, the column temperature was set to 20 °C with an injection volume of 5 μL. The spray, cone, extractor, and RF lens voltages were at 4 kV, 30 V, 8, and 2 V, respectively. The source and desolvation temperatures were set to 120 and 350 °C, respectively, and the desolvation gas flow was set to 750 L/h. Data analysis was conducted using MassLynx 4.1 software (Waters Corporation, Milford, MA, USA).

Absorption, distribution, metabolism, and excretion studies

EXPERIMENTAL ANIMALS.

All animal experiments were carried out in accordance with German law and associated animal experimentation licenses. 7- to 11-week-old C57B6 female mice were purchased from Janvier Laboratories and maintained in a specific-pathogen-free animal facility. They were kept for at least 7 days after arrival for acclimatization. To reduce the number of animals per experiment, *n* was chosen to be 3 per group. Body weights were approximately 22 g per mouse, with each mouse being weighed before treatment to ensure equal doses for all animals.

FORMULATIONS FOR USE IN VIVO.

Treatment solutions were freshly prepared before the start of each study. For i.v. treatment, compounds were dissolved in DMSO and then diluted 20-fold in cognate female serum (final DMSO concentration 5%) 0.2 mg/mL 7p for application at 5 mL/ kg to reach a dose of 1 mg/kg per substance. The vehicle for

Published in : Journal of Agricultural and Food Chemistryl (2024), vol. 72, n°37, pp. 20670-20678
DOI: 10.1021/acs.jafc.4c05094
Status : Postprint (Author's version)

p.o. treatment comprised 2% v/v Tween 80, 20% v/v PEG 400, 1 mM citric acid, qsp 0,5% w/v HPMC 2 mg/mL 7p. The solutions were thoroughly homogenized via a vortex mixer and ultrasonic bath.

COLLECTION OF SAMPLES.

To measure drug concentrations in plasma, blood was collected from mice tail vein at different time points. In the group of mice treated with i.v. injections, blood was collected 20, 60, 120 and 240 min after treatment. In the group of mice treated p.o., blood was collected 20, 60, 120, 240 and 480 min after treatment. Animals were sacrificed after 4 or 8 h by CO_2 inhalation. Brain, liver, and spleen, as well as cardiac blood was collected in heparinized tubes and centrifuged for 8 min at 8000 rpm at 4 °C. The supernatant was used to determine plasma concentrations. Both plasma and organ samples were immediately stored at −25 °C until workup for analysis.

SAMPLE WORKUP FOR HPLC−MS.

Plasma samples were diluted with 6 volumes of acetonitrile containing 1 nM terbuthylazine (internal standard). Organ samples were treated with 1 μL of proteinase K solution (0.5 mg/mL in 20 mM phosphate buffer) per mg organ weight and then homogenized in a FastPrep FP-120 instrument and then centrifuged at 14,000 rpm for 7 min at 4 °C.

SAMPLE ANALYSIS.

Compound concentrations were measured using reverse-phase HPLC with MSMS detection. The procedure used a mobile phase comprising 0.1% formic acid in water (solvent A) and 0.1% formic acid in acetonitrile (solvent B). Method: 10% B for 1 min, to 100% B in 1 min, 100% B for 3 min, to 10% B in 1 min, 10% B for 2 min, stop time 8 min, flow rate 500 μL/min, injection volume 6 μL. Using a thermostat, a constant column temperature of 45 °C was maintained, while the samples were kept at 6 °C. MS parameters were optimized with authentic standards in positive ionization mode based on a fragment with the highest molecular weight and the highest sensitivity.

CALCULATION OF PLASMA HALF-LIFE.

Half-lives of compounds in mice were calculated using the plasma concentrations measured with the aforementioned methods. To reduce the influence of distribution processes, plasma concentrations before t = 15 min were not included. Values outside the quantification limits were disregarded for the calculation of the elimination constants and resulting half-lives.

Published in : Journal of Agricultural and Food Chemistryl (2024), vol. 72, n°37, pp. 20670-20678
DOI: 10.1021/acs.jafc.4c05094
Status : Postprint (Author's version)

MOLECULAR MODELING.

HOMOLOGY MODELS.

Homology models of full-length GPR27 (UniProt: Q9NS67) were generated using I-TASSER.[33] I-TASSER selected a series of ten templates for the modeling based on the primary and secondary structure similarity. The top five generated homology models were visually inspected for folding, displaying differences only in the C-terminal region (amino acid number 356−371). Superimposition of the final model with the top five selected templates shows a variation in the RMSD ranging from 1.11 to 2.10 Å, where major disagreements between model-templates reside in the intracellular regions and not the TM helices. Therefore, the model with the highest *C*-value (−0.49) was chosen for further validation. *C*values range from −5 to 2, where the highest value represents the model with the highest confidence. The selected GPR27 model was evaluated by geometry and Ramachandran plot (calculated using MolProbity[34]), where it displayed 24 residues as Ramachandran outliers and 16 residues as poor rotamers. Thus, the model underwent energy minimization to fix those problems before docking.

The human *β*-arrestin-2 (UniProt: P32121) was modeled using the mice *β*-arrestin coordinates (PDB ID: 5W0P[24]) as a template. GPR27-*β*-arrestin models were assembled by superimposing the individual models in the 5W0P orientation. Final models were generated by manually adding the relevant phosphorylation sites followed by a step of local energy minimization using Maestro (2021v4, OPLS4 force-field, steep descent 1 Å cutoff).

MOLECULAR DOCKING.

All ligands for docking were drawn using Maestro and prepared using LigPrep to generate the three-dimensional conformation, adjust the protonation state to physiological pH (7.4), and calculate the partial atomic charges, with the force field OPLS4. Docking studies with the prepared ligands were performed using Glide (Glide V7.7), with the flexible modality of Induced-fit docking[35,36] with extra precision, followed by a side-chain minimization step using Prime. Ligands were docked within a grid around 13 Å from the centroid of the orthosteric pocket, identified using SiteMap (Schrödinger LCC[37]), generating ten poses per ligand. Docking poses were visually inspected, independently from the docking score, and the ones with the highest number of consistent interactions were selected for simulation.

MOLECULAR DYNAMICS SIMULATIONS.

The GPR27-*β*-arrestin model with the 7p or 7ab ligand was simulated to clarify which residues contributed to the stability within the binding site. Molecular dynamics (MD) simulations were carried out using the Desmond engine[38] with the OPLS4 force-field.[39] The simulated system encompassed the protein−ligand/cofactor complex, a predefined water model (TIP3P[40]) as a solvent, counterions (Na^+ or Cl^- adjusted to neutralize the overall system charge) plus enough to simulate a concentration of 150 mM and a POPC membrane, which was positioned based on the transmembrane motifs determined in the model. The system was treated in an orthorhombic box with periodic boundary conditions specifying the shape and the size of the box as 10 × 10 × 13 Å distance from the box edges to any atom of the protein. Short-

Published in : Journal of Agricultural and Food Chemistryl (2024), vol. 72, n°37, pp. 20670-20678
DOI: 10.1021/acs.jafc.4c05094
Status : Postprint (Author's version)

range Coulombic interactions were performed using time steps of 1 fs and a cutoff value of 9.0 Å, whereas long-range Coulombic interactions were handled using the Smooth Particle Mesh Ewald method.[41] GPR27 + ligands systems were then subjected to simulations of 200 ns for equilibration purposes, but only for 7p the last frame was used to generate new replicas. The equilibrated system underwent at least 1.3 μs, in four-five replicas, followed by analysis to characterize the protein−ligand interaction. The results of the simulations, in the form of trajectory and interaction data, are available on the Zenodo repository (code: 10.5281/zenodo.7022576). MD trajectories were visualized, and figures were produced using PyMOL v.2.5.2 (Schrödinger LCC, New York, NY, USA).

Molecular Dynamics Simulation Analyses.

Protein−ligand interactions and distances were determined using the Simulation Event Analysis pipeline implemented using the software Maestro 2021v.4 (Schrödinger LCC). Protein− protein interactions were analyzed using the script analyze_trajectory_ppi.py also provided by Schrödinger (LCC). Molecular mechanics energies with generalized the compounds' binding energy was calculated using the Born and surface area continuum solvation (MM/GBSA) model, using Prime[42] and the implemented thermal MM/GBSA script. For the calculations, each 10th frame of MD was used. Finally, root-mean-square deviation (RMSD) values of the protein backbone were used to monitor simulation equilibration and protein changes. The fluctuation (RMSF) by residues was calculated using the initial MD frame as a reference and compared between ligand-bound and apo structure simulations (files available in the Zenodo repository). Protein−protein interactions between relevant elements are depicted in the Supporting Information, Tables S1−S3.

Associated content

DATA AVAILABILITY STATEMENT

The results of the simulations, in the form of trajectory and interaction data, are available on the Zenodo repository (code: 10.5281/zenodo.7022576), which will be available upon publication.

* SUPPORTING INFORMATION

The Supporting Information is available free of charge at https://pubs.acs.org/doi/10.1021/acs.jmedchem.3c02030.

Interaction frequency between GPR27's C-terminal and the β-arrestin interface; GPR27-β-arrestin interaction frequency with relevant amino acids; phosphate frequency interaction; metabolic stability of 7p in HLM and MLM; evaluation of 7p and 7af cytotoxicity; and 1H and 13C NMR Spectra and the HPLC traces of selected compounds (PDF)

Coordinates of homology models and ligand-bound docking (1077_5k_conf1) (PDB)

Published in : Journal of Agricultural and Food Chemistryl (2024), vol. 72, n°37, pp. 20670-20678
DOI: 10.1021/acs.jafc.4c05094
Status : Postprint (Author's version)

Coordinates of homology models and ligand-bound docking (1077_5k_conf2) (PDB)

Coordinates of homology models and ligand-bound docking (1079_5k_conf1 (2)) (PDB)

Molecular formula strings and the associated biological data (CSV)

Author Contributions

T.P. and M.W. contributed equally.

NOTES

The authors declare no competing financial interest.

Acknowledgments

TüCAD2 is funded by the Federal Ministry of Education and Research (BMBF) and the Baden-Württemberg Ministry of Science as part of the Excellence Strategy of the German Federal and State Governments. T.K. was supported by the Fortüne initiative (no. 2613-0-0) and by the iFIT, which are both initiatives from the Excellence Strategy of the German Federal and State Governments. The authors would like to thank the CSC-Finland for the generous computational resources. C.S. and A.-D.L. are supported by the Deutsche Forschungsgemeinschaft-Project-ID 407707190, the SFB1423 and the Pre-Doc Award of Leipzig University. The authors thank Petra Krumbholz for technical assistance. J. Hanson is a F.R.S.-FNRS senior research associate and was supported by a research project grant from the F.R.S.-FNRS (PDRT.0111.19). The authors thank Kristine Schmidt for proofreading (language).

Abbreviations

β_2AR, adrenoceptor; BRET, bioluminescence resonance energy transfer; cAMP, cyclic adenosine monophosphate; DMSO, dimethyl sulfoxide; DCM, dichloromethane; ESIMS, electrospray ionization mass spectrometry; GPCR, G proteincoupled receptor; HLM, human liver microsome; HRMS, high-resolution mass spectrometry; HPLC, high-performance liquid chromatography; IUPHAR, International Union of Basic and Clinical Pharmacology; MLM, muse liver microsome; MDS, molecular dynamic simulation; MP, melting point; NMR, nuclear magnetic resonance; PDB, protein data bank; SREB, super conserved receptors expressed in the brain; SAR, structure–activity relationship; TM, transmembrane; TLC, thin layer chromatography; THF, tetrahydrofuran

Published in : Journal of Agricultural and Food Chemistryl (2024), vol. 72, n°37, pp. 20670-20678
DOI: 10.1021/acs.jafc.4c05094
Status : Postprint (Author's version)

References

(1) Alexander, S. P.; Christopoulos, A.; Davenport, A. P.; Kelly, E.; Mathie, A.; Peters, J. A.; Veale, E. L.; Armstrong, J. F.; Faccenda, E.; Harding, S. D.; Pawson, A. J.; Southan, C.; Davies, J. A.; Abbracchio, M. P.; Alexander, W.; Al-Hosaini, K.; Bäck, M.; Barnes, N. M.; Bathgate, R.; Beaulieu, J.-M.; Bernstein, K. E.; Bettler, B.; Birdsall, N. J. M.; Blaho, V.; Boulay, F.; Bousquet, C.; Bräuner-Osborne, H.; Burnstock, G.; Caló, G.; Castaño, J. P.; Catt, K. J.; Ceruti, S.; Chazot, P.; Chiang, N.; Chini, B.; Chun, J.; Cianciulli, A.; Civelli, O.; Clapp, L. H.; Couture, R.; Csaba, Z.; Dahlgren, C.; Dent, G.; Singh, K. D.; Douglas, S. D.; Dournaud, P.; Eguchi, S.; Escher, E.; Filardo, E. J.; Fong, T.; Fumagalli, M.; Gainetdinov, R. R.; Gasparo, M. d.; Gerard, C.; Gershengorn, M.; Gobeil, F.; Goodfriend, T. L.; Goudet, C.; Gregory, K. J.; Gundlach, A. L.; Hamann, J.; Hanson, J.; Hauger, R. L.; Hay, D. L.; Heinemann, A.; Hollenberg, M. D.; Holliday, N. D.; Horiuchi, M.; Hoyer, D.; Hunyady, L.; Husain, A.; Ijzerman, A. P.; Inagami, T.; Jacobson, K. A.; Jensen, R. T.; Jockers, R.; Jonnalagadda, D.; Karnik, S.; Kaupmann, K.; Kemp, J.; Kennedy, C.; Kihara, Y.; Kitazawa, T.; Kozielewicz, P.; Kreienkamp, H.-J.; Kukkonen, J. P.; Langenhan, T.; Leach, K.; Lecca, D.; Lee, J. D.; Leeman, S. E.; Leprince, J.; Li, X. X.; Williams, T. L.; Lolait, S. J.; Lupp, A.; Macrae, R.; Maguire, J.; Mazella, J.; McArdle, C. A.; Melmed, S.; Michel, M. C.; Miller, L. J.; Mitolo, V.; Mouillac, B.; Müller, C. E.; Murphy, P.; Nahon, J.-L.; Ngo, T.; Norel, X.; Nyimanu, D.; O'Carroll, A.-M.; Offermanns, S.; Panaro, M. A.; Parmentier, M.; Pertwee, R. G.; Pin, J.P.; Prossnitz, E. R.; Quinn, M.; Ramachandran, R.; Ray, M.; Reinscheid, R. K.; Rondard, P.; Rovati, G. E.; Ruzza, C.; Sanger, G. J.; Schöneberg, T.; Schulte, G.; Schulz, S.; Segaloff, D. L.; Serhan, C. N.; Stoddart, L. A.; Sugimoto, Y.; Summers, R.; Tan, V. P.; Thal, D.; Thomas, W. W.; Timmermans, P. B. M. W. M.; Tirupula, K.; Tulipano, G.; Unal, H.; Unger, T.; Valant, C.; Vanderheyden, P.; Vaudry, D.; Vaudry, H.; Vilardaga, J.-P.; Walker, C. S.; Wang, J. M.; Ward, D. T.; Wester, H.-J.; Willars, G. B.; Woodruff, T. M.; Yao, C.; Ye, R. D. THE CONCISE GUIDE TO PHARMACOLOGY 2021/ 22: G Protein-Coupled Receptors. *Br. J. Pharmacol.* 2021, *178*, S27− S156.

(2) Hauser, A. S.; Attwood, M. M.; Rask-Andersen, M.; Schiöth, H. B.; Gloriam, D. E. Trends in GPCR Drug Discovery: New Agents, Targets and Indications. *Nat. Rev. Drug Discov.* 2017, *16* (12), 829− 842.

(3) Sriram, K.; Insel, P. A. G Protein-Coupled Receptors as Targets for Approved Drugs: How Many Targets and How Many Drugs? *Mol. Pharmacol.* 2018, *93* (4), 251−258.

(4) Laschet, C.; Dupuis, N.; Hanson, J. The G Protein-Coupled Receptors Deorphanization Landscape. *Biochem. Pharmacol.* 2018, *153*, 62−74.

(5) Davenport, A. P.; Alexander, S. P. H.; Sharman, J. L.; Pawson, A. J.; Benson, H. E.; Monaghan, A. E.; Liew, W. C.; Mpamhanga, C. P.; Bonner, T. I.; Neubig, R. R.; Pin, J. P.; Spedding, M.; Harmar, A. J. International Union of Basic and Clinical Pharmacology. LXXXVIII. G Protein-Coupled Receptor List: Recommendations for New Pairings with Cognate Ligands. *Pharmacol. Rev.* 2013, *65* (3), 967− 986.

(6) Roth, B. L.; Kroeze, W. K. Integrated Approaches for GenomeWide Interrogation of the Druggable Non-Olfactory G ProteinCoupled Receptor Superfamily. *J. Biol. Chem.* 2015, *290* (32), 19471−19477.

(7) Edwards, A. M.; Isserlin, R.; Bader, G. D.; Frye, S. V.; Willson, T. M.; Yu, F. H. Too Many Roads Not Taken. *Nature* 2011, *470* (7333), 163−165.

(8) Stäubert, C.; Wozniak, M.; Dupuis, N.; Laschet, C.; Pillaiyar, T.; Hanson, J. Superconserved Receptors Expressed in the Brain: Expression, Function, Motifs and Evolution of an Orphan Receptor Family. *Pharmacol. Ther.* 2022, *240*, 108217.

Published in : Journal of Agricultural and Food Chemistryl (2024), vol. 72, n°37, pp. 20670-20678
DOI: 10.1021/acs.jafc.4c05094
Status : Postprint (Author's version)

(9) Bayrak, A.; Hanson, J.; Laufer, S.; Pillaiyar, T. Super-Conserved Receptors Expressed in the Brain: Biology and Medicinal Chemistry Efforts. *Future Med. Chem.* 2022, *14* (12), 899−913.

(10) Matsumoto, M.; Saito, T.; Takasaki, J.; Kamohara, M.; Sugimoto, T.; Kobayashi, M.; Tadokoro, M.; Matsumoto, S.; Ohishi, T.; Furuichi, K. An Evolutionarily Conserved G-Protein Coupled Receptor Family, SREB, Expressed in the Central Nervous System. *Biochem. Biophys. Res. Commun.* 2000, *272* (2), 576−582.

(11) Regard, J. B.; Sato, I. T.; Coughlin, S. R. Anatomical Profiling of G Protein-Coupled Receptor Expression. *Cell* 2008, *135* (3), 561− 571.

(12) Ku, G. M.; Pappalardo, Z.; Luo, C. C.; German, M. S.; McManus, M. T. An siRNA Screen in Pancreatic Beta Cells Reveals a Role for Gpr27 in Insulin Production. *PLoS Genet.* 2012, *8* (1), No. e1002449.

(13) Chopra, D. G.; Yiv, N.; Hennings, T. G.; Zhang, Y.; Ku, G. M. Deletion of Gpr27 in Vivo Reduces Insulin mRNA but Does Not Result in Diabetes. *Sci. Rep.* 2020, *10* (1), 5629.

(14) Breton, T. S.; Sampson, W. G. B.; Clifford, B.; Phaneuf, A. M.; Smidt, I.; True, T.; Wilcox, A. R.; Lipscomb, T.; Murray, C.; DiMaggio, M. A. Characterization of the G Protein-Coupled Receptor Family SREB across Fish Evolution. *Sci. Rep.* 2021, *11* (1), 12066.

(15) Nath, A. K.; Ma, J.; Chen, Z.-Z.; Li, Z.; Vitery, M. D. C.; Kelley, M. L.; Peterson, R. T.; Gerszten, R. E.; Yeh, J.-R. J. Genetic Deletion of Gpr27 Alters Acylcarnitine Metabolism, Insulin Sensitivity, and Glucose Homeostasis in Zebrafish. *FASEB J.* 2020, *34* (1), 1546− 1557.

(16) Dolanc, D.; Zorec, T. M.; Smole, Z.; Maver, A.; Horvat, A.; Pillaiyar, T.; Trkov Bobnar, S.; Vardjan, N.; Kreft, M.; Chowdhury, H. H.; Zorec, R. The Activation of GPR27 Increases Cytosolic L-Lactate in 3T3 Embryonic Cells and Astrocytes. *Cells* 2022, *11* (6), 1009.

(17) Dupuis, N.; Laschet, C.; Franssen, D.; Szpakowska, M.; Gilissen, J.; Geubelle, P.; Soni, A.; Parent, A.-S.; Pirotte, B.; Chevigné, A.; Twizere, J.-C.; Hanson, J. Activation of the Orphan G ProteinCoupled Receptor GPR27 by Surrogate Ligands Promotes β-Arrestin 2 Recruitment. *Mol. Pharmacol.* 2017, *91* (6), 595−608.

(18) Pillaiyar, T.; Rosato, F.; Wozniak, M.; Blavier, J.; Charles, M.; Laschet, C.; Kronenberger, T.; Müller, C. E.; Hanson, J. StructureActivity Relationships of Agonists for the Orphan G Protein-Coupled Receptor GPR27. *Eur. J. Med. Chem.* 2021, *225*, 113777.

(19) Ge, S.; Zhong, H.; Ma, X.; Zheng, Y.; Zou, Y.; Wang, F.; Wang, Y.; Hu, Y.; Li, Y.; Liu, W.; Guo, W.; Xu, Q.; Lai, Y. Discovery of Secondary Sulphonamides as IDO1 Inhibitors with Potent Antitumour Effects in Vivo. *J. Enzyme Inhib. Med. Chem.* 2020, *35* (1), 1240−1257.

(20) Xu, F.; Zhao, Y.; Zhou, H.; Li, C.; Zhang, X.; Hou, T.; Qu, L.; Wei, L.; Wang, J.; Liu, Y.; Liang, X. Synthesis and Evaluation of 3-(4(Phenoxymethyl)Phenyl)Propanoic Acid and N-Phenylbenzenesulfonamide Derivatives as FFA4 Agonists. *Bioorg. Med. Chem. Lett.* 2020, *30* (24), 127650.

(21) Silveira, F. F.; de Souza, J. O.; Hoelz, L. V. B.; Campos, V. R.; Jabor, V. A. P.; Aguiar, A. C. C.; Nonato, M. C.; Albuquerque, M. G.; Guido, R. V. C.; Boechat, N.; Pinheiro, L. C. S. Comparative Study between the Anti-P. Falciparum Activity of Triazolopyrimidine, Pyrazolopyrimidine and Quinoline Derivatives and the Identification of New PfDHODH Inhibitors. *Eur. J. Med. Chem.* 2021, *209*, 112941.

Published in : Journal of Agricultural and Food Chemistryl (2024), vol. 72, n°37, pp. 20670-20678
DOI: 10.1021/acs.jafc.4c05094
Status : Postprint (Author's version)

(22) Batra, N.; Rajendran, V.; Agarwal, D.; Wadi, I.; Ghosh, P. C.; Gupta, R. D.; Nath, M. Synthesis and Antimalarial Evaluation of [1, 2,3]-Triazole-Tethered Sulfonamide-Berberine Hybrids. *ChemistrySelect* 2018, *3* (34), 9790−9793.

(23) Kroeze, W. K.; Sassano, M. F.; Huang, X.-P.; Lansu, K.; McCorvy, J. D.; Giguerè, P. M.; Sciaky, N.; Roth, B. L. PRESTOTango as an Open-Source Resource for Interrogation of the Druggable Human GPCRome. *Nat. Struct. Mol. Biol.* 2015, *22* (5), 362−369.

(24) Zhou, X. E.; He, Y.; de Waal, P. W.; Gao, X.; Kang, Y.; Van Eps, N.; Yin, Y.; Pal, K.; Goswami, D.; White, T. A.; Barty, A.; Latorraca, N. R.; Chapman, H. N.; Hubbell, W. L.; Dror, R. O.; Stevens, R. C.; Cherezov, V.; Gurevich, V. V.; Griffin, P. R.; Ernst, O. P.; Melcher, K.; Xu, H. E. Identification of Phosphorylation Codes for Arrestin Recruitment by G Protein-Coupled Receptors. *Cell* 2017, *170* (3), 457−469.e13.

(25) Pandey, S.; Kumari, P.; Baidya, M.; Kise, R.; Cao, Y.; DwivediAgnihotri, H.; Banerjee, R.; Li, X. X.; Cui, C. S.; Lee, J. D.; Kawakami, K.; Maharana, J.; Ranjan, A.; Chaturvedi, M.; Jhingan, G. D.; Laporte, S. A.; Woodruff, T. M.; Inoue, A.; Shukla, A. K. Intrinsic Bias at NonCanonical, *β*-Arrestin-Coupled Seven Transmembrane Receptors. *Mol. Cell* 2021, *81* (22), 4605−4621.e11.

(26) Jang, W.; Lu, S.; Xu, X.; Wu, G.; Lambert, N. A. The Role of G Protein Conformation in Receptor-G Protein Selectivity. *Nat. Chem. Biol.* 2023, *19*, 687−694.

(27) Liebing, A.-D.; Krumbholz, P.; Stäubert, C. Protocol to Characterize Gi/o and Gs Protein-Coupled Receptors in Transiently Transfected Cells Using ELISA and cAMP Measurements. *STAR Protoc.* 2023, *4* (1), 102120.

(28) Gilissen, J.; Geubelle, P.; Dupuis, N.; Laschet, C.; Pirotte, B.; Hanson, J. Forskolin-Free cAMP Assay for Gi-Coupled Receptors. *Biochem. Pharmacol.* 2015, *98* (3), 381−391.

(29) Schihada, H.; Shekhani, R.; Schulte, G. Quantitative Assessment of Constitutive G Protein-Coupled Receptor Activity with BRET-Based G Protein Biosensors. *Sci. Signal.* 2021, *14* (699), No. eabf1653.

(30) Wang, L.; Li, L.; Zhou, Z.-H.; Jiang, Z.-Y.; You, Q.-D.; Xu, X.-L. Structure-Based Virtual Screening and Optimization of Modulators Targeting Hsp90-Cdc37 Interaction. *Eur. J. Med. Chem.* 2017, *136*, 63−73.

(31) Ahad, A. Md.; Zuohe, S.; Du-Cuny, L.; Moses, S. A.; Zhou, L. L.; Zhang, S.; Powis, G.; Meuillet, E. J.; Mash, E. A. Development of Sulfonamide AKT PH Domain Inhibitors. *Bioorg. Med. Chem.* 2011, *19* (6), 2046−2054.

(32) Li, J.; Chen, J.; Gui, C.; Zhang, L.; Qin, Y.; Xu, Q.; Zhang, J.; Liu, H.; Shen, X.; Jiang, H. Discovering Novel Chemical Inhibitors of Human Cyclophilin A: Virtual Screening, Synthesis, and Bioassay. *Bioorg. Med. Chem.* 2006, *14* (7), 2209−2224.

(33) Roy, A.; Kucukural, A.; Zhang, Y. I-TASSER: A Unified Platform for Automated Protein Structure and Function Prediction. *Nat. Protoc.* 2010, *5* (4), 725−738.

(34) Chen, V. B.; Arendall, W. B.; Headd, J. J.; Keedy, D. A.; Immormino, R. M.; Kapral, G. J.; Murray, L. W.; Richardson, J. S.; Richardson, D. C. MolProbity: All-Atom Structure Validation for Macromolecular Crystallography. *Acta Crystallogr., Sect. D: Biol. Crystallogr.* 2010, *66* (1), 12−21.

(35) Sherman, W.; Beard, H. S.; Farid, R. Use of an Induced Fit Receptor Structure in Virtual Screening. *Chem. Biol. Drug Des.* 2006, *67* (1), 83−84.

Published in : Journal of Agricultural and Food Chemistryl (2024), vol. 72, n°37, pp. 20670-20678
DOI: 10.1021/acs.jafc.4c05094
Status : Postprint (Author's version)

(36) Friesner, R. A.; Banks, J. L.; Murphy, R. B.; Halgren, T. A.; Klicic, J. J.; Mainz, D. T.; Repasky, M. P.; Knoll, E. H.; Shelley, M.; Perry, J. K.; Shaw, D. E.; Francis, P.; Shenkin, P. S. Glide: A New Approach for Rapid, Accurate Docking and Scoring. 1. Method and Assessment of Docking Accuracy. *J. Med. Chem.* 2004, *47* (7), 1739− 1749.

(37) Halgren, T. A. Identifying and Characterizing Binding Sites and Assessing Druggability. *J. Chem. Inf. Model.* 2009, *49* (2), 377−389.

(38) Bowers, K. J.; Chow, E.; Xu, H.; Dror, R. O.; Eastwood, M. P.; Gregersen, B. A.; Klepeis, J. L.; Kolossvary, I.; Moraes, M. A.; Sacerdoti, F. D.; Salmon, J. K.; Shan, Y.; Shaw, D. E. Scalable Algorithms for Molecular Dynamics Simulations on Commodity Clusters. *SC '06: Proceedings of the 2006 ACM/IEEE Conference on Supercomputing*; ACM: New York, NY, USA, 2006.

(39) Lu, C.; Wu, C.; Ghoreishi, D.; Chen, W.; Wang, L.; Damm, W.; Ross, G. A.; Dahlgren, M. K.; Russell, E.; Von Bargen, C. D.; Abel, R.; Friesner, R. A.; Harder, E. D. OPLS4: Improving Force Field Accuracy on Challenging Regimes of Chemical Space. *J. Chem. Theory Comput.* 2021, *17* (7), 4291−4300.

(40) Jorgensen, W. L.; Chandrasekhar, J.; Madura, J. D.; Impey, R. W.; Klein, M. L. Comparison of Simple Potential Functions for Simulating Liquid Water. *J. Chem. Phys.* 1983, *79* (2), 926−935.

(41) Darden, T.; York, D.; Pedersen, L. Particle mesh Ewald: An *N*· log(*N*) method for Ewald sums in large systems. *J. Chem. Phys.* 1993, *98* (12), 10089−10092.

(42) Jacobson, M. P.; Pincus, D. L.; Rapp, C. S.; Day, T. J. F.; Honig, B.; Shaw, D. E.; Friesner, R. A. A Hierarchical Approach to All-Atom Protein Loop Prediction. *Proteins* 2004, *55* (2), 351−367.